Modeling and Comparison of Passive Component Volume of Hybrid Resonant Switched-Capacitor Converters

Zichao Ye, *Graduate Student Member, IEEE*, Seth R. Sanders, *Fellow, IEEE*, and Robert Carl Nikolai Pilawa-Podgurski, *Senior Member, IEEE*

***Abstract*—Hybrid and resonant switched-capacitor (SC) converters enable efficient utilization of both active and passive components, and have the potential to achieve higher efficiency and higher power density than conventional SC and magnetic-based converters. One or more added inductors offer an additional degree of freedom in the design space. It is of great interest to understand the tradeoffs between capacitor and inductor size and volume allocation. In this article, we analyze the reactive energy processed by the passive components and use it to calculate the total passive component volume. It is shown that the total passive component volume of resonant SC (ReSC) converters can be expressed as a function of flying capacitor voltage ripple, and the optimized capacitor voltage ripple that minimizes the total volume is dependent on topology specific parameters and the relative energy density ratio between capacitors and inductors. Moreover, we also demonstrate through theoretical analysis and experimentation that ReSC converters use significantly less passive component volume than conventional SC and buck converters for the same amount of power converted. Next, to compare different ReSC topologies, a normalized passive volume parameter is proposed for simple and fair comparison. This can be used along with a normalized switch stress parameter (based on switch VA ratings) to create a framework to showcase the relative performance of different topologies. This framework can be used to visualize and compare the passive and active component utilization among different topologies. Additionally, the proposed reactive power analysis is extended to hybrid converters with regulation capability.**

***Index Terms*—DC–DC converter, hybrid converter, multilevel converter, passive component, reactive energy, resonant, switched capacitor (SC), topology.**

Manuscript received October 8, 2021; revised January 9, 2022; accepted March 2, 2022. Date of publication March 18, 2022; date of current version May 23, 2022. An earlier version of this paper was presented in part at the 2019 Workshop on Control and Modeling for Power Electronics (COMPEL) [DOI: 10.1109/COMPEL.2019.8769707]. This manuscript includes more design guidelines for engineering practice, new analysis and comparison with pure switched-capacitor converters, experimental verification, as well as analysis of regulated hybrid converters. The information, data, or work presented herein was funded in part by the Advanced Research Projects Agency-Energy (ARPA-E), U.S. Department of Energy, under Award Number DE-AR0000906 in the CIRCUITS program monitored by Dr. Isik Kizilyalli. The views and opinions of authors expressed herein do not necessarily state or reflect those of the United States Government or any agency thereof. Recommended for publication by Associate Editor C.-J. Chen. *(Corresponding author: Robert Carl Nikolai Pilawa-Podgurski.)*

The authors are with the Department of Electrical Engineering and Computer Sciences, University of California, Berkeley, CA 94720 USA (e-mail: yezichao@berkeley.edu; sanders@eecs.berkeley.edu; pilawa@berkeley.edu).

Color versions of one or more figures in this article are available at https://doi.org/10.1109/TPEL.2022.3160675.

Digital Object Identifier 10.1109/TPEL.2022.3160675

I. Introduction

HYBRID and resonant switched-capacitor (SC) converters [1]–[7] have received increased attention lately, owing to superior efficiency and power density compared to conventional SC and magnetic based converters. The added inductor(s) can help reduce or eliminate the capacitor charge sharing loss present in pure SC converters through soft-charging operation [8]–[12], thereby allowing larger capacitor voltage ripple and better capacitor energy utilization. However, depending on the relative energy density of the inductors and capacitors, it is unclear whether the capacitor volume reduction can offset the volume of the augmenting inductor and lead to a smaller overall volume than that of a pure SC converter. Moreover, as the augmenting inductors offer an additional degree of freedom in the design space, it is crucial to evaluate and find the optimum inductor and capacitor allocation that minimizes the total passive component volume. In this article, we approach this problem from the perspective of the fundamental reactive energy/power processed by the passive components. It is found that the total passive component volume of resonant SC (ReSC) converters can be expressed as a function of flying capacitor voltage ripple, and the optimized capacitor voltage ripple that minimizes the total volume is dependent on the topology specific parameters and the relative energy density ratio between capacitor and inductor. We also experimentally demonstrate that ReSC converters use significantly less passive volume than conventional SC and buck converters for the same amount of power converted, while maintaining the best efficiency performance.

The proposed reactive energy/power analysis can also provide direct passive volume comparison among different ReSC topologies. Given fixed output power and switching frequency, the passive volume of each topology can be normalized and expressed as a function that consists of only topology-dependent parameters and the relative energy density of inductors and capacitors. Combining with the classical switch total VA rating metric, which reflects potential efficiency, we provide a simple yet powerful framework to evaluate the relative performance (active and passive component utilization) of various ReSC topologies. Moreover, the theoretical lower-bound limits of passive and active components are derived to identify the framework boundaries such that any new emerging topologies can be analyzed and incorporated into the comparison space.

This article extends an earlier conference publication [13] of this work. Here, we present more detailed analysis and design guidelines to facilitate practical ReSC converter designs. We also provide an in-depth comparison between ReSC converters and pure SC converters and highlight the favored operating condition of each type. Three hardware prototypes are designed and implemented to compare the 2-to-1 ReSC converter with the pure SC converter and the buck converter. Additionally, the proposed reactive power analysis is extended to hybrid converters with regulation capability.

The rest of this article is organized as follows. In Section II, the proposed reactive energy analysis methodology is introduced and demonstrated on a 2-to-1 ReSC converter. Based on this analysis, a number of observations and design guidelines is derived to facilitate practical ReSC converter designs in Section III. Next, the proposed reactive energy analysis is generalized to arbitrary ReSC topologies in Section IV and a simple yet powerful framework to evaluate the relative performance (in terms of active and passive component utilization) of different ReSC topologies is presented in Section V. In Section VI, with the examples of a three-level buck converter and a series-capacitor buck converter, the proposed reactive power analysis is extended to hybrid converters with regulation capability. Finally, Section VII concludes this article.

II. Analysis of Basic 2-to-1 ReSC Converter

The volume of a passive component is directly related to the peak energy it can store, as well as its type and technology. In ReSC converters, the resonant inductors are able to transfer all stored energy as the sinusoidal or rectified sinusoidal inductor current reaches zero at each switching state. In contrast, each flying capacitor can typically only deliver a portion of its stored energy, which is determined by the magnitude of its voltage ripple on top of the dc average voltage. To calculate the total passive component volume of ReSC converters, we propose an energy-based method by fundamentally analyzing the reactive energy/power processed by the passive components. Note that the term "reactive power" is also referred to as "indirect power" in [14] and [15]. Here, we use the basic 2-to-1 ReSC converter as an example to demonstrate the proposed method. The reactive energy processed by the flying capacitor and the resonant inductor is first calculated. Then, this processed energy is related to the required stored energy through an energy utilization factor. Finally, the passive component volume is derived by dividing the required stored energy by the energy density of the corresponding passive components. It will be shown that the total passive volume can be expressed and subsequently optimized as a function of the flying capacitor voltage ripple ratio.

The schematic drawing of a 2-to-1 ReSC converter and its two operating states are shown in Fig. 1. All switches have a fixed duty ratio of 50%, and there is a 180° phase shift between the "A" switches and the "B" switches. The switching frequency is the resonant frequency of the flying capacitor and the inductor ($f_{\text{sw}} = \frac{\omega_r}{2\pi} = \frac{1}{2\pi\sqrt{LC}}$), as it is the minimum frequency with full soft-charging for hybrid SC converters [11]. The switching period T is $T = \frac{1}{f_{\text{sw}}}$. As shown in Fig. 2, the flying capacitor has

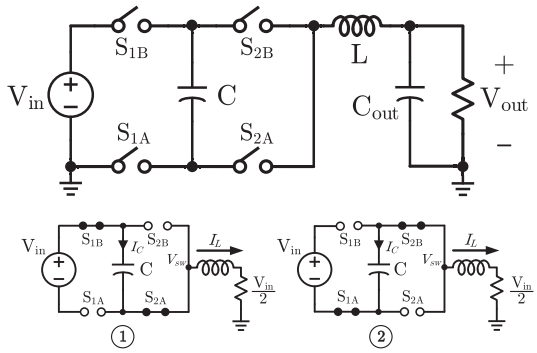

Fig. 1. Schematic drawing of a 2-to-1 resonant SC converter and its two operating states.

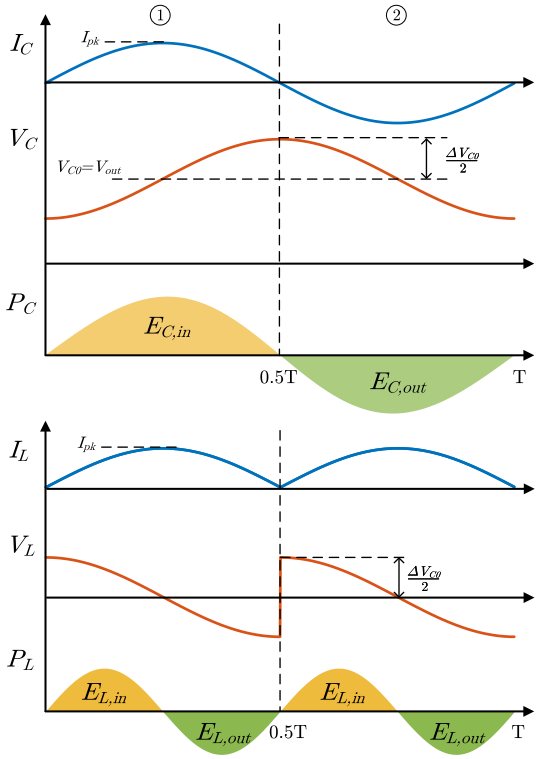

Fig. 2. Current, voltage, and power waveforms of the flying capacitor and the resonant inductor in a 2-to-1 ReSC converter.

a sinusoidal current $I_C = I_{pk}\sin(\omega_r t)$, and the corresponding capacitor voltage has a dc component of $V_{C0} = V_{\text{out}}$ and an ac component of $-\frac{I_{pk}}{C\omega_r}\cos(\omega_r t)$, with a peak-to-peak ripple voltage of $\Delta V_{C0} = \frac{2I_{pk}}{C\omega_r}$. In contrast, the inductor current is a rectified sine wave with the same amplitude as that of the capacitor current, and the voltage across the inductor has the same peak magnitude as the capacitor voltage ripple, but at twice the frequency. By multiplying the current and the voltage waveforms, the instantaneous power processed by the capacitor $V_C(t)I_C(t)$ and the inductor $V_L(t)I_L(t)$ can be derived as shown in Fig. 2, and the shaded areas represent the energy flowing into and out of the passive component in each cycle.

Here, we define the concept of "reactive energy processed" by a passive component. In periodic steady state, the net energy

flowing into a passive component is zero under the assumption of lossless energy transfer, i.e., the energy flowing in, E_{in}, at one (or a few consecutive) operating state(s) equals the energy flowing out, E_{out}, at the next (or the next few consecutive) operating state(s). The reactive energy processed by a passive component, E_{process}, is the *maximum* amount of energy that is cyclically stored and delivered, i.e., $E_{\text{process}} = E_{\text{in}} = E_{\text{out}}$.

For the 2-to-1 ReSC converter in Fig. 2, $E_{C,\text{in}}$ is the energy flowing into the flying capacitor at the first half switching cycle. At the second half cycle, the same amount of energy, $E_{C,\text{out}}$, flows out of the capacitor. Therefore, the reactive energy processed by the flying capacitor $E_{C,\text{process}}$ can be calculated as

$$\begin{aligned} E_{C,\text{process}} &= E_{C,\text{in}} = E_{C,\text{out}} \\ &= \int_0^{\frac{T}{2}} I_c(t)V_c(t)dt \\ &= \int_0^{\frac{T}{2}} I_{pk}\sin(\omega_r t)\left(V_{\text{out}} - \frac{I_{pk}}{C\omega_r}\cos(\omega_r t)\right)dt \\ &= \frac{T}{2}V_{\text{out}}I_{\text{out}} \end{aligned} \tag{1}$$

where $I_{\text{out}} = \frac{2}{\pi}I_{pk}$ is the average output current.

The resonant inductor in the 2-to-1 ReSC converter sees doubled frequency compared to the flying capacitor. It alternately stores and delivers energy twice per switching cycle. As a result, when calculating its processed reactive energy $E_{L,\text{process}}$, which is *the maximum amount of energy that is being cyclically used*, we only need to consider one energy in or out state and the corresponding period is $\frac{T}{4}$

$$\begin{aligned} E_{L,\text{process}} &= E_{L,\text{in}} = E_{L,\text{out}} \\ &= \int_0^{\frac{T}{4}} I_L(t)V_L(t)dt \\ &= \int_0^{\frac{T}{4}} I_{pk}\sin(\omega_r t)\frac{I_{pk}}{C\omega_r}\cos(\omega_r t)dt \\ &= \frac{T^2 I_{\text{out}}^2}{32\,C}. \end{aligned} \tag{2}$$

To gain more insights, we next introduce the concept of "reactive power rating" of a passive component. For a passive element k, its reactive power rating is defined as $P_k = \frac{E_{k,\text{process}}}{T}$. By factoring out the operating dependent term T, we get a power rating metric P_k similar to the switch VA rating metric, which reflects the intrinsic property of the topology. For the 2-to-1 ReSC converter, the reactive power rating of the flying capacitor and the resonant inductor are derived to be

$$\begin{aligned} P_{C0} &= \frac{E_{C,\text{process}}}{T} \\ &= \frac{1}{2}V_{\text{out}}I_{\text{out}} \\ P_{L0} &= \frac{E_{L,\text{process}}}{T} \\ &= \frac{TI_{\text{out}}^2}{32\,C} \\ &= \frac{I_{\text{out}}^2}{32Cf_{\text{sw}}}. \end{aligned} \tag{3, 4}$$

Equation (4) can be further expressed as a function of flying capacitor voltage ripple ratio. By substituting in the average-to-peak capacitor voltage ripple $\frac{1}{2}\Delta V_{C0} = \frac{I_{pk}}{C\omega_r} = \frac{I_{\text{out}}}{4Cf_{\text{sw}}}$, we get

$$P_{L0} = \frac{I_{\text{out}}\Delta V_{C0}}{16} = \frac{P_{\text{out}}}{16}\cdot\frac{\Delta V_{C0}}{V_{\text{out}}} = \frac{P_{\text{out}}}{16}\cdot\frac{\Delta V_{C0}}{V_{C0}} \tag{5}$$

where $V_{C0} = V_{\text{out}}$ is the dc average voltage of the flying capacitor.

A side note is that the definition of reactive power rating here is slightly different from the Wolaver definition on [16, p. 63]. Instead of considering the maximum amount of energy that is being *cyclically* used (e.g., there are two energy transfer cycles per switching period for the inductor in the 2-to-1 ReSC converter, but we only calculate the processed energy of one cycle), Wolaver focused on the *total* amount of energy that needs to be *transferred* by the passive component per switching cycle, and therefore defined the reactive power of a reactive element k to be $P_k = \frac{1}{2}\cdot\frac{1}{T}\int_0^T \mid V_k I_k \mid dt$. This definition would lead to a result that is twice that of (4) for the resonant inductor.

In conjunction with the "indirect power" concept in [14], the proposed reactive power rating metric can be used to evaluate the efficacy of passive component utilization of a topology. As discussed in [14], the indirect power P_{ind} that needs to be processed by a converter with a gain of G ($G = \frac{V_{\text{in}}}{V_{\text{out}}}$ for a step-down converter) is governed by $P_{\text{ind}} \geq \frac{G-1}{G}P_{\text{out}}$. For any 2-to-1 converters, $P_{\text{ind}} \geq \frac{1}{2}P_{\text{out}}$. In the 2-to-1 ReSC case, $P_{C0} = \frac{1}{2}P_{\text{out}}$ and $P_{L0} = \frac{P_{\text{out}}}{16}\cdot\frac{\Delta V_{C0}}{V_{C0}}$. The same concept will also be used to analyze regulated hybrid converters in Section VI.

Now that we have derived the reactive energy processed by the passive components and the corresponding reactive power ratings, we can next calculate the total energy that needs to be stored by these passive components. For the flying capacitor, the processed reactive energy $E_{C,\text{process}}$ equals the difference between the peak and minimum stored energy per switching cycle

$$\begin{aligned} E_{C,\text{process}} &= \frac{1}{2}C\left[\left(V_{C0}+\frac{1}{2}\Delta V_{C0}\right)^2 - \left(V_{C0}-\frac{1}{2}\Delta V_{C0}\right)^2\right] \\ &= CV_{C0}\Delta V_{C0}. \end{aligned} \tag{6}$$

Then, we define the energy utilization factor of the capacitor as the ratio of its reactive energy processed per cycle and the peak energy that is stored

$$\mu_C = \frac{E_{C,\text{process}}}{E_{C,\text{store}}} = \frac{CV_{C0}\Delta V_{C0}}{\frac{1}{2}C(V_{C0}+\frac{1}{2}\Delta V_{C0})^2} = \frac{2\frac{\Delta V_{C0}}{V_{C0}}}{(1+\frac{1}{2}\frac{\Delta V_{C0}}{V_{C0}})^2}. \tag{7}$$

For a fixed amount of processed energy, a higher μ_C indicates a lower stored energy and smaller capacitor size, and vice versa. The capacitor volume Vol_C can be expressed with respect to its processed energy as

$$\text{Vol}_\text{C} = \frac{E_{C,\text{store}}}{\rho_{E,C}} = \frac{\frac{E_{C,\text{process}}}{\mu_C}}{\rho_{E,C}} = \frac{\frac{P_{C0}}{f_{\text{sw}}\mu_C}}{\rho_{E,C}} \tag{8}$$

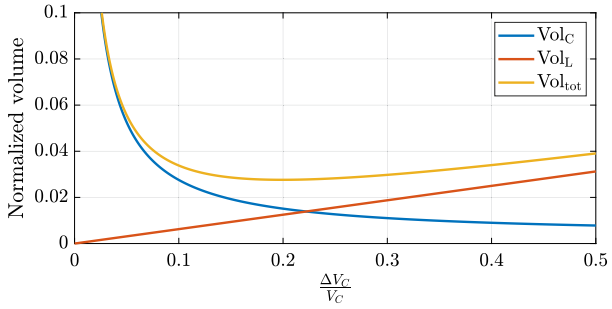

Fig. 3. Effects of flying capacitor voltage ripple on capacitor volume, inductor volume, and overall volume of a 2-to-1 ReSC converter (assuming $\rho_{E,C}/\rho_{E,L} = 100$).

where $\rho_{E,C}$ is the energy density of the capacitor; it is physically limited by the energy density capability of the dielectric material.

For the resonant inductor, the rectified sinusoidal current reaches zero every half cycle. Thus, the inductor processed energy equals the stored energy (i.e., its energy utilization factor $\mu_L = 1$) and

$$\mathrm{Vol_L} = \frac{E_{L,\mathrm{store}}}{\rho_{E,L}} = \frac{E_{L,\mathrm{process}}}{\rho_{E,L}} = \frac{\frac{P_{L0}}{f_{\mathrm{sw}}}}{\rho_{E,L}} \tag{9}$$

where $\rho_{E,L}$ is the energy density of the inductor; it is physically limited by a number of factors, such as the magnetic core structure (i.e., gapped and nongapped), the maximum flux density and loss density of the magnetic material, etc.

Revisiting (3) and (5), it can be observed that the reactive power rating of the capacitor is fixed for a given output power. Moreover, it can be shown that this value is equal to the power rating of the flying capacitor in a pure 2-to-1 SC converter. Even though the augmenting inductor does not change the power/energy that is processed by the flying capacitor, it allows unconstrained capacitor voltage ripple $\frac{\Delta V_{C0}}{V_{C0}}$ without efficiency penalty through resonant soft-charging operation, and therefore improves the energy utilization factor of the flying capacitor and results in a smaller capacitor volume. However, the capacitor volume reduction comes at a cost. As shown in (5), the reactive power rating of the inductor is an increasing function of $\frac{\Delta V_{C0}}{V_{C0}}$, which leads to an increase in the inductor volume (9) when the capacitor volume is reduced. The effects of $\frac{\Delta V_{C0}}{V_{C0}}$ on capacitor volume and inductor volume are plotted in Fig. 3, assuming $\rho_{E,C}/\rho_{E,L} = 100$.

The tradeoff between the capacitor volume and the inductor volume can be observed more clearly from the total passive component volume

$$\begin{aligned}\mathrm{Vol_{tot}} &= \mathrm{Vol_C} + \mathrm{Vol_L} \\ &= \frac{P_{\mathrm{out}}}{f_{\mathrm{sw}}}\left(\frac{\frac{1}{4}\left(1+\frac{V_{C0}}{\Delta V_{C0}}+\frac{\Delta V_{C0}}{4V_{C0}}\right)}{\rho_{E,C}} + \frac{\frac{1}{16}\frac{\Delta V_{C0}}{V_{C0}}}{\rho_{E,L}}\right)\end{aligned} \tag{10}$$

where $\mathrm{Vol_C}$ is primarily a function of $\frac{V_{C0}}{\Delta V_{C0}}$, whereas $\mathrm{Vol_L}$ is a function of $\frac{\Delta V_{C0}}{V_{C0}}$. For a given set of P_{out}, f_{sw}, $\rho_{E,C}$, and $\rho_{E,L}$, (10) can be differentiated with respect to the capacitor ripple ratio $\frac{\Delta V_{C0}}{V_{C0}}$ to find the optimum ratio $(\frac{\Delta V_{C0}}{V_{C0}})^*$ that minimizes the total volume

$$\frac{d\mathrm{Vol_{tot}}}{\frac{\Delta V_{C0}}{V_{C0}}} = 0 \Longrightarrow \left(\frac{\Delta V_{C0}}{V_{C0}}\right)^* = \sqrt{\frac{4\rho_{E,L}}{\rho_{E,L}+\rho_{E,C}}} \approx 2\sqrt{\frac{\rho_{E,L}}{\rho_{E,C}}}. \tag{11}$$

It can be seen that $(\frac{\Delta V_{C0}}{V_{C0}})^*$ is inversely proportional to $\sqrt{\frac{\rho_{E,C}}{\rho_{E,L}}}$. When $\frac{\rho_{E,C}}{\rho_{E,L}}$ increases, $(\frac{\Delta V_{C0}}{V_{C0}})^*$ decreases, corresponding to a passive component allocation with more capacitance and less inductance.

Substituting (11) into (10), the minimized total passive volume of a 2-to-1 ReSC converter is given by

$$\mathrm{Vol_{tot,min}} \approx \frac{P_{\mathrm{out}}}{f_{\mathrm{sw}}\rho_{E,L}}\left(\frac{\frac{\rho_{E,L}}{\rho_{E,C}}+\sqrt{\frac{\rho_{E,L}}{\rho_{E,C}}}}{4}\right). \tag{12}$$

Note that the above analysis assumes the passive components are ideal and lossless. A number of loss factors associated with the passive components, such as capacitor equivalent series resistance (ESR) loss [17], inductor dc resistance (DCR) and ac resistance (ACR) losses and core loss [18] are not considered here. These loss factors will have additional impact on the optimum capacitor ripple ratio and size allocation, and the results may differ for applications with different voltage and power levels. In the next section, the above theoretical analysis will be used to derive guidelines for practical designs, followed by experimental verification.

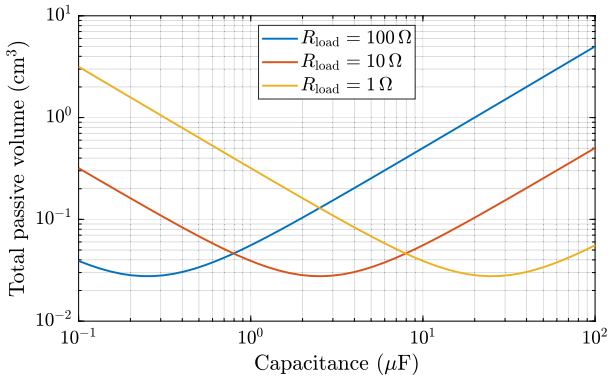

Fig. 4. Given fixed output power and switching frequency, the 2-to-1 ReSC converter can always achieve the same minimum total passive component volume. But the optimum capacitance (and inductance) allocation depends on the magnitude of the load resistance. Parameters for the plot: $P_{\mathrm{out}} = 100$ W, $f_{\mathrm{sw}} = 100$ kHz, $\rho_{E,C} = 0.1$ J/cm^3, $\rho_{E,C}/\rho_{E,L} = 100$.

III. Design Guidelines and Comparisons With Other Solutions

A. Design Guidelines

Given fixed output power and switching frequency, the total passive component volume of the 2-to-1 ReSC converter is plotted in Fig. 4 with respect to flying capacitance. It can be seen from this impedance scaling plot that, regardless of the magnitude of the load resistance R_{load}, the ReSC converter can always achieve the same minimized total passive component

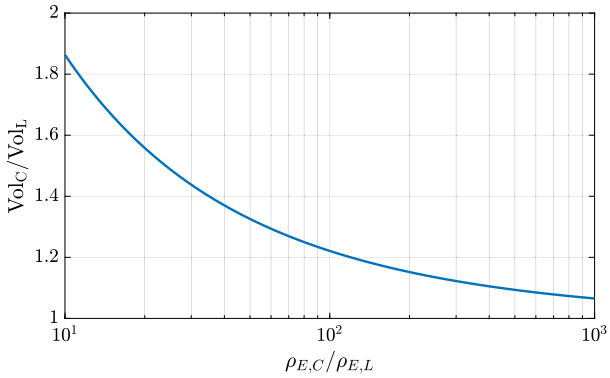

Fig. 5. Optimum volume ratio between capacitor and inductor with respect to their energy density ratio.

volume, which is derived in (12). The optimum flying capacitance that provides the lowest total passive volume is inversely dependent on the load resistance. It indicates that, with fixed output power and switching frequency, higher capacitance (and lower inductance) should be used for applications with lower output voltage and higher output current. This is based on the fact that, given fixed nominal capacitance and inductance values, the capacitor volume depends on the voltage rating, while the inductor volume depends on the current rating. The capacitor and inductor volume that give the minimized total volume can be calculated by substituting the optimized capacitor ripple ratio $(\frac{\Delta V_{C0}}{V_{C0}})^*$ of (11) into (8) and (9), respectively. Fig. 5 plots the optimized volume ratio with respect to the energy density ratio between capacitor and inductor. Within a practical range of $100 \leq \rho_{E,C}/\rho_{E,L} \leq 1000$, the optimum volume ratio is slightly greater than 1, indicating that the flying capacitor and the resonant inductor should have similar volume. Note that even though this analysis is based on the assumption of lossless passive components, the result matches with the finding in [18] and [19], where the optimized passive component allocation is derived for minimized total power loss.

B. Comparison With Buck Converter

Now that we have derived the minimized total passive component volume of a 2-to-1 ReSC converter, it is of great interest to compare the result with other types of converters, such as magnetic-based converters. Since both the inductor in a buck converter and the transformer in a transformer-bridge converter have similar volt–second product requirements, the size of their respective magnetic components will be similar [20]. Here, we calculate the minimum required inductor size of a buck converter at 2-to-1 conversion ratio, with the same output power and switching frequency as that of the ReSC converter.

To maximize the inductor energy utilization factor μ_L, a buck converter should operate at the boundary conduction mode (BCM), which describes the operating condition at the boundary of continuous conduction mode (CCM) and discontinuous conduction mode (DCM). At BCM, the inductor current ripple is twice the average current. Consequently, the inductor current reaches zero every switching cycle and the inductor is able to transfer all of its stored energy per switching cycle, i.e., its energy utilization factor is maximized ($\mu_L = 1$). It is also shown that BCM operation may be desired from efficiency perspective as it can result in minimal total power loss especially for integrated applications [21].

As derived in [16], the reactive power rating of the inductor is $P_{L0} = \frac{1}{2}P_{\text{out}}$, when the duty ratio D is 0.5. Assuming BCM operation where the inductor stored energy equals its processed energy, the minimized volume of the inductor of a buck converter at a given P_{out} and f_{sw} can be found to be

$$\mathrm{Vol}_{\mathrm{L,buck}} = \frac{\frac{1}{2}P_{\text{out}}}{f_{\text{sw}}\rho_{E,L}}. \tag{13}$$

Comparing with (12), it can be seen that the minimized total passive volume of the 2-to-1 ReSC converter is 1.2 times that of a 2-to-1 buck converter when $\rho_{E,C} = \rho_{E,L}$. In order for the ReSC converter to achieve a smaller volume than that of a buck converter, we need $\rho_{E,C} \gg \rho_{E,L}$. For instance, if $\rho_{E,C} = 100\rho_{E,L}$, the volume of the ReSC converter is 0.055 times that of the buck converter.

Note that this comparison is based on the assumption that all passive components in the ReSC converter and the buck converter are lossless. In practice, the buck inductor is more lossy than the LC tank of the ReSC converter as will be shown in the experimental verification section. Therefore, this ideal lossless comparison disadvantages the ReSC converter compared to the buck converter as their potential efficiency performance are not taken into consideration.

C. Comparison With Pure SC Converter

Compared to a pure SC converter, the augmenting inductor of the ReSC converter can help eliminate the capacitor charge sharing loss and therefore allow higher capacitor voltage ripple without degrading the efficiency. However, depending on the relative energy density of inductor and capacitor, it is unclear whether the capacitor volume reduction can offset the volume of the augmenting inductor and lead to a smaller overall volume than that of a pure SC converter.

Here, we compare the relative passive component volume of the 2-to-1 ReSC converter and the 2-to-1 pure SC converter. It can be easily shown that the reactive power rating of the flying capacitor of a 2-to-1 pure SC converter is the same as that in the ReSC case: $P_C = \frac{1}{2}P_{\text{out}}$. However, its minimized total passive volume cannot be derived with the same method. This is because there is no inductor to constrain its flying capacitor voltage ripple ratio $\frac{\Delta V_C}{V_C}$, and thus its energy utilization factor μ_C is unconstrained and can be as large as 1. Nevertheless, unlike the ReSC converter in which the capacitor voltage ripple and the power loss are decoupled because of soft-charging operation, the pure SC converter suffers from capacitor charge sharing loss, which is dependent on the capacitor voltage ripple ratio. Therefore, in order to have a relatively fair volume comparison, care should be taken to ensure the pure SC converter operates under a similar condition and has comparable efficiency performance when comparing with the ReSC converter.

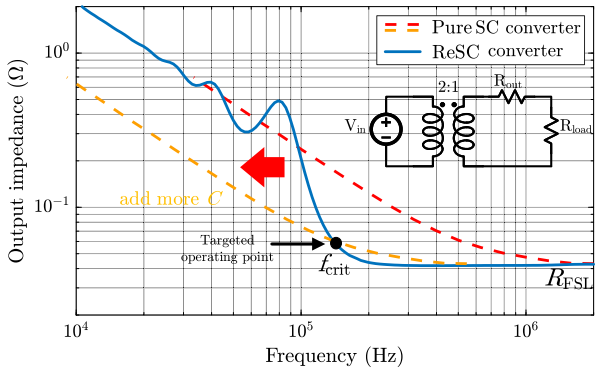

Fig. 6. Output impedance of 2-to-1 Pure SC and ReSC converters vs. frequency.

SC converters can be modeled by an ideal transformer [22]. The output impedance at the secondary side of the transformer is a good indication of the efficiency performance. In Fig. 6, the simulated output impedance of 2-to-1 pure SC converter and 2-to-1 ReSC converter are plotted in red and blue, respectively. It is assumed that both converters have the same flying capacitance and series resistance (e.g., switch on-resistance and capacitor ESR). The additional DCR and ACR of the augmenting inductor in the ReSC converter are not considered here. It can be seen from Fig. 6 that both converters approach the same lowest possible output impedance R_{FSL} at the fast switching limit (FSL) region, which is solely determined by the series resistance in the circuit [22]. With an augmenting inductor, the ReSC converter can approach R_{FSL} at a much lower switching frequency. As derived in [23], when operating at the resonant frequency $f_{\text{crit}} = \frac{1}{2\pi\sqrt{LC}}$, the output impedance of the ReSC converter is

$$R_{\text{out,ReSC}} = \frac{\pi^2}{8} R_{\text{FSL}}. \tag{14}$$

In contrast, [23] also shows that the output impedance of 2-to-1 pure SC converter with respect to its switching frequency f_{sw} and flying capacitance C_p is

$$R_{\text{out,pureSC}} = \frac{coth\left(\frac{1}{4R_{\text{FSL}}C_p f_{\text{sw}}}\right)}{4C_p f_{\text{sw}}}. \tag{15}$$

To keep the comparison simple and straightforward, an assumption is made here that both converters operate at the same switching frequency so that their switching losses are approximately the same. The switching frequency is selected to be the resonant frequency of the ReSC converter f_{crit}:

$$f_{\text{sw}} = f_{\text{crit}} = \frac{1}{2\pi\sqrt{LC}} \tag{16}$$

where L and C are the resonant inductance and flying capacitance of the 2-to-1 ReSC converter. It is worth noting that this fixed frequency assumption cannot guarantee an overall optimum design, as the switching frequency is an important design knob to maximize efficiency and power density [18], [24] and needs to be carefully selected based on the voltage and power rating of an application.

In order to have comparable overall efficiency, the two converters should also be designed to have approximately the same output impedance at f_{crit}. As illustrated in Fig. 6, this can be achieved by reducing the output impedance of the pure SC converter with more capacitance (from the red curve to the yellow curve). By equating (14) and (15), we get

$$C_p \approx \frac{1}{3.43 R_{\text{FSL}} f_{\text{sw}}}. \tag{17}$$

For the simplicity of the following derivation, the numerical constant in (17) is substituted with $\zeta = 3.43$:

$$C_p \approx \frac{1}{\zeta R_{\text{FSL}} f_{\text{sw}}}. \tag{18}$$

Now we calculate the 2-to-1 pure SC converter volume, $\text{Vol}_{\text{pureSC}}$, based on its peak stored energy and the energy density of the capacitor, $\rho_{E,C}$:

$$\text{Vol}_{\text{pureSC}} = \frac{\frac{1}{2}C_p(V_o + \frac{1}{2}\Delta V_o)^2}{\rho_{E,C}}. \tag{19}$$

Its peak-to-peak capacitor voltage ripple ΔV_o can be expressed as

$$\Delta V_o = \frac{\Delta q_{\text{in}}}{C_p} = \frac{I_{\text{in}} T}{C_p} = \frac{\frac{P_{\text{out}}}{2V_o} T}{C_p} = \frac{P_{\text{out}}}{2 f_{\text{sw}} V_o C_p}. \tag{20}$$

By substituting (18) and (20) into (19), we get

$$\text{Vol}_{\text{pureSC}} = \frac{\left(V_o + \frac{\zeta P_{\text{out}} R_{\text{FSL}}}{4V_o}\right)^2}{2\zeta \rho_{E,C} f_{\text{sw}} R_{\text{FSL}}}. \tag{21}$$

Next, dividing (21) by (12) yields the relative volume ratio:

$$\frac{\text{Vol}_{\text{pureSC}}}{\text{Vol}_{\text{ReSC}}} = \frac{\left(4 + \frac{\zeta R_{\text{FSL}}}{R_{\text{load}}}\right)^2}{8\zeta \frac{R_{\text{FSL}}}{R_{\text{load}}}\left(1 + \sqrt{\frac{\rho_{E,C}}{\rho_{E,L}}}\right)} \tag{22}$$

where $R_{\text{load}} = \frac{V_o^2}{P_{\text{out}}}$ is the output load resistance. It can be seen that the relative volume ratio is dependent on not only the energy density ratio of capacitor and inductor $\sqrt{\frac{\rho_{E,C}}{\rho_{E,L}}}$, but also the ratio of the converter's series resistance and the load resistance $\frac{R_{\text{FSL}}}{R_{\text{load}}}$. To better illustrate the effect of $\frac{R_{\text{FSL}}}{R_{\text{load}}}$, we can express the relative volume ratio with respect to converter efficiency. Based on the ideal transformer model [22], the efficiency of SC converters is given by

$$\eta = \frac{R_{\text{load}}}{R_{\text{out}} + R_{\text{load}}}. \tag{23}$$

As shown in (14), $R_{\text{out}} = \frac{\pi^2}{8} R_{\text{FSL}}$ at the desired resonant operating point and therefore

$$\eta = \frac{R_{\text{load}}}{\frac{\pi^2}{8} R_{\text{FSL}} + R_{\text{load}}}. \tag{24}$$

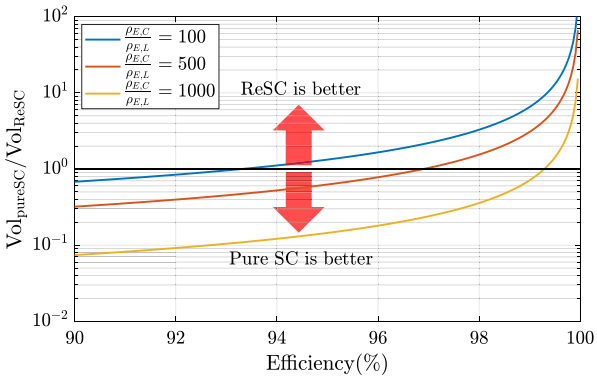

Fig. 7. Relative passive component volume comparison between 2-to-1 pure SC converter and 2-to-1 ReSC converter with respect to converter efficiency. Only conduction loss is considered.

Thus, $\frac{R_{\mathrm{FSL}}}{R_{\mathrm{load}}}$ can be written as $\frac{R_{\mathrm{FSL}}}{R_{\mathrm{load}}} = \frac{8}{\pi^2}(\frac{1}{\eta} - 1)$ and (22) is equivalent to

$$\frac{\mathrm{Vol_{pureSC}}}{\mathrm{Vol_{ReSC}}} = \frac{\left(4 + \frac{8\zeta}{\pi^2}\left(\frac{1}{\eta} - 1\right)\right)^2}{\frac{64\zeta}{\pi^2}\left(\frac{1}{\eta} - 1\right)\left(1 + \sqrt{\frac{\rho_{E,C}}{\rho_{E,L}}}\right)}. \tag{25}$$

This way, we are able to directly observe the relationship between achievable efficiency and passive component volume of the two approaches as plotted in Fig. 7. For a practical value of $\frac{\rho_{E,C}}{\rho_{E,L}} = 100$ for discrete passive devices, the 2-to-1 ReSC converter can have a smaller volume than the pure SC case when the designed efficiency is greater than 93.3%. However, for very low-voltage high-current applications, such efficiency number might be unreachable due to the limit of $\frac{R_{\mathrm{FSL}}}{R_{\mathrm{load}}}$ and pure SC converters could be a better choice. Note that this analysis assumes the ReSC converter and the pure SC converter have the same series resistance, including switch on-resistance and capacitor ESR. In practice, the series resistance of the ReSC converter may be higher due to the additional DCR/ACR of the resonant inductor as well as the slightly higher capacitor ESR since the ReSC converter uses less capacitance. This may favor the pure SC converter in a broader state space than that shown in Fig. 7.

Another perspective to approach this problem is the quality factor Q of the resonant tank of the ReSC converter. For the 2-to-1 ReSC converter, $\Delta V_{C0} = \frac{I_{\mathrm{out}}}{2Cf_{\mathrm{sw}}}$ and $V_{C0} = V_{\mathrm{out}}$, so we can express $\frac{\Delta V_{C0}}{V_{C0}}$ as

$$\frac{\Delta V_{C0}}{V_{C0}} = \frac{I_{\mathrm{out}}}{2Cf_{\mathrm{sw}}V_{\mathrm{out}}} = \frac{1}{2Cf_{\mathrm{sw}}R_{\mathrm{load}}}. \tag{26}$$

Substituting (26) into (11), the optimal $(\frac{\Delta V_{C0}}{V_{C0}})^*$ that minimizes the total passive component volume, we get

$$\frac{1}{2Cf_{\mathrm{sw}}R_{\mathrm{load}}} = \sqrt{\frac{4\rho_{E,L}}{\rho_{E,L} + \rho_{E,C}}}. \tag{27}$$

Assuming $\rho_{E,C} \gg \rho_{E,L}$ and using $L = \frac{1}{4\pi^2 f_{\mathrm{sw}}^2 C}$, (27) can be written as

$$\frac{2\pi^2 f_{\mathrm{sw}} L}{R_{\mathrm{load}}} \approx 2\sqrt{\frac{\rho_{E,L}}{\rho_{E,C}}}. \tag{28}$$

With the quality factor of the resonant tank being $Q = \frac{2\pi f_{\mathrm{sw}} L}{R_{\mathrm{FSL}}}$, the optimal quality factor Q^* that corresponds to a 2-to-1 ReSC converter with minimized total passive component volume is derived to be

$$Q^* \approx \frac{2}{\pi}\frac{R_{\mathrm{load}}}{R_{\mathrm{FSL}}}\sqrt{\frac{\rho_{E,L}}{\rho_{E,C}}}. \tag{29}$$

As disccused in [25], a practical constraint of Q in order for the ReSC converter to outperform the pure SC converter, i.e., achiving lower output impedance at the resonant frequency, can be found from the output impedance ratio of the two converters:

$$\frac{R_{\mathrm{out,pureSC}}}{R_{\mathrm{out,ReSC}}} = \frac{4}{\pi}Q > 1 \tag{30}$$

which requires $Q > \frac{\pi}{4}$. Combining it with (29) yields another design requirement to build a reasonable ReSC converter that could better its pure SC counterpart:

$$\frac{R_{\mathrm{load}}}{R_{\mathrm{FSL}}}\sqrt{\frac{\rho_{E,L}}{\rho_{E,C}}} > \frac{\pi^2}{8}. \tag{31}$$

It can be concluded from (30) and (31) that there are several situations where ReSC converters cannot perform better than pure SC converters:

1) The resonant tank is inherently incapable to achieve a Q that is greater than $\frac{\pi}{4}$ so that the ReSC converter cannot have a lower output impedance compared to a pure SC converter with the same flying capacitance. Due to the fundamental scaling of magnetics, this can be the case when the physical size of the inductor is small, e.g., in milimeter scale and below.
2) The physical size and material of the inductor are not limiting factors in terms of achievable Q. However, a small $\frac{R_{\mathrm{load}}}{R_{\mathrm{FSL}}}$ ratio dictates that the optimum Q^* could be less than $\frac{\pi}{4}$, resulting in no performance benefits over a pure SC converter operating with the same flying capacitance and switching frequency. This effect can also be observed from Fig. 4, which shows that given fixed P_{out} and f_{sw}, a design with smaller R_{load} needs a larger capacitance and a smaller inductance, leading to a reduction of Q. Therefore, for applications with small R_{load}, such as low-voltage high-current CPU power delivery, the ReSC design requires extra careful analysis to make sure the augmenting inductor could provide efficiency and power density improvments. The important design factors that are not considered in the model above include the losses incured by the inductor, the optimum switch sizing and operating frequency, etc.

D. Experimental Verification

Three hardware prototypes are designed to investigate the above passive volume analysis and comparison. As can be seen from Fig. 8, there are three 2-to-1 converters on the board,

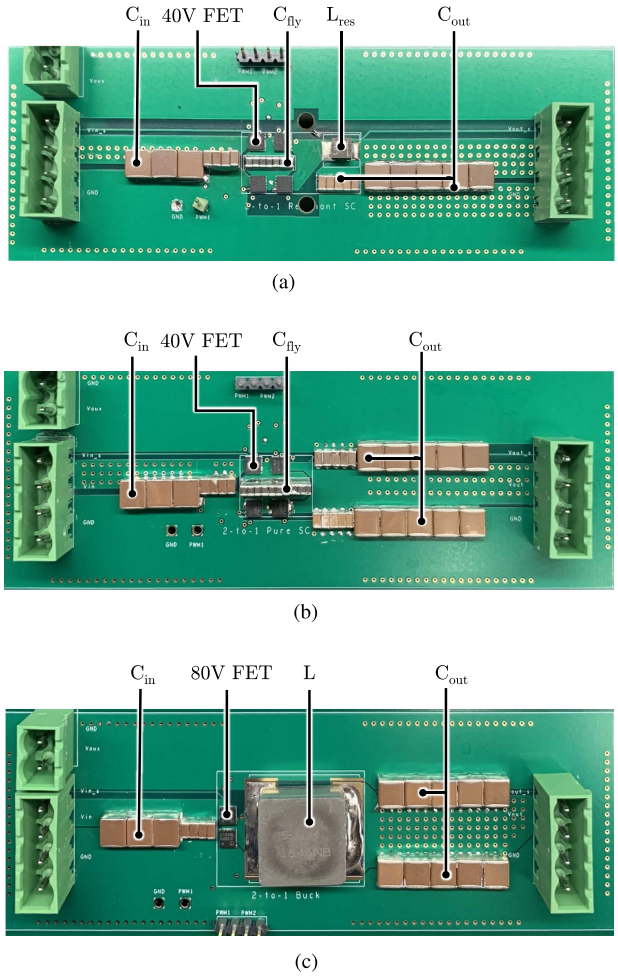

Fig. 8. Photograph of the three hardware prototypes for passive component volume and efficiency comparison. (a) 2-to-1 ReSC. (b) 2-to-1 Pure SC. (c) 2-to-1 Buck.

TABLE I
KEY CONVERTER PARAMETERS

Input voltage	48 V
Output voltage	24 V
Output current	15 A
Power rating	360 W
Switching frequency	100 kHz

including an ReSC converter, a pure SC converter and a buck converter. They share the same operating parameters shown in Table I. Since the efficiency analysis of SC converters in the last subsection mainly considers conduction loss, a relatively low switching frequency of 100 kHz and a high output current of 15 A are selected here to make sure the converters operate at heavy-load region and are conduction-loss dominated.

The major active and passive components of the converters are highlighted in Fig. 8, and their parameters are tabulated in Table II. Sufficient filtering capacitances are used to ensure negligible effect of input and output voltage ripples on efficiency performance. The modeling and analysis of SC converters with finite terminal capacitances can be found in [26]. For the ReSC converter, given a desired resonant frequency of 100 kHz, the resonant inductor and capacitor are selected as follows. First, the inductor should be able to use all of its stored energy (i.e., its energy utilization factor is $\mu_L = 1$). This requires that the peak inductor current should be close to its saturation point: $I_{\text{sat}} \approx I_{\text{pk}} = \frac{\pi}{2} I_{\text{out}}$. Under this constraint, an inductor with lower profile is desired. However, in order to not degrade the efficiency significantly, the inductor DCR should be comparable to or lower than the equivalent total switch on-resistance. Second, as illustrated in Fig. 5, a volume ratio $\frac{\text{Vol}_\text{C}}{\text{Vol}_\text{L}}$ close to one is more likely to minimize the total passive component volume. This principle can be used to guide the L and C allocation. After evaluating the available commercial components, 200 nH Coilcraft XEL4030 inductor is selected for its good balance of volume and loss, and 35V-0805-X5R TDK ceramic capacitors are selected as the flying capacitors. Besides very high energy density, the selected capacitors also have small package size which allows for fine tuning the total flying capacitance. The selected LC tank has an energy density ratio of $\frac{\rho_{E,C}}{\rho_{E,L}} = 233$, a total volume of 76 mm^3 and a volume ratio of $\frac{\text{Vol}_\text{C}}{\text{Vol}_\text{L}} = 0.6$. Note that this $\frac{\text{Vol}_\text{C}}{\text{Vol}_\text{L}}$ slightly deviates from the theoretical optimum due to the limited selection of inductor size.

The pure SC converter uses the same switches and flying capacitors as those of the ReSC converter. Given same power rating and switching frequency, its efficiency can be controlled by the amount of flying capacitance. In order to compare the required passive volume with the ReSC converter, an efficiency sweep is performed repeatedly with an increasing amount of flying capacitance, until the pure SC converter can achieve the same efficiency performance as that of the ReSC converter at 15 A output current. The measured efficiency performance is shown in Fig. 9. It is found that the pure SC converter needs 272 mm^3 of flying capacitors to match the efficiency of the ReSC converter. This results in a volume ratio $\frac{\text{Vol}_\text{pureSC}}{\text{Vol}_\text{ReSC}}$ of 3.6, as compared to a calculated value of 4.4. The deviation is possibly from the additional loss of the resonant inductor, which is not considered in the model.

For the buck converter, it is very challenging to achieve 99% efficiency at this operating point. Therefore, the comparison of its passive volume is mainly focused on the minimal energy storage requirement, rather than comparable efficiency performance. By performing inductor volt-second analysis, it can be found that when converting 48 to 24 V at 100 kHz, a minimum 4 μH inductance is needed to maintain boundary conduction mode at 15 A output current. Among available off-the-shelf inductors, the Vishay IHLP6767 family is found to be a good candidate that can meet both the inductance and saturation current requirements. The selected inductor has 5.6 μH and 40 A saturation current, and thus a total energy storage greater than the minimum requirement. It has a volume of 2059 mm^3 and an energy density ratio $\frac{\rho_{E,C}}{\rho_{E,L}}$ of 94 with respect to the flying capacitor in SC-based converters. Note that the energy density of this buck inductor is different and higher than that of the resonant inductor in the ReSC converter. Based on (12) and (13), the theoretical volume ratio is found to be $\frac{\text{Vol}_\text{buck}}{\text{Vol}_\text{ReSC}} = 11.5$.

TABLE II
MAIN COMPONENT LISTING OF THE HARDWARE PROTOTYPE

	Component	Part number	Parameters
ReSC	Switch	Infineon BSZ018N04LS6	40 V, 1.6 mΩ
	Flying capacitor	TDK C2012X5R1V226M125AC	X5R, 35 V, 22 μF*$\times$9
	Resonant inductor	XEL4030-201ME	200 nH, 22 A I_{sat}
Pure SC	Switch	Infineon BSZ018N04LS6	40 V, 1.6 mΩ
	Flying capacitor	TDK C2012X5R1V226M125AC	X5R, 35 V, 22 μF*$\times$87
Buck	Switch	Infineon BSZ070N08LS5	80 V, 5.9 mΩ
	Inductor	Vishay IHLP6767GZER5R6M01	5.6 μH, 40 A I_{sat}

*The capacitance listed here is the nominal value before dc derating.

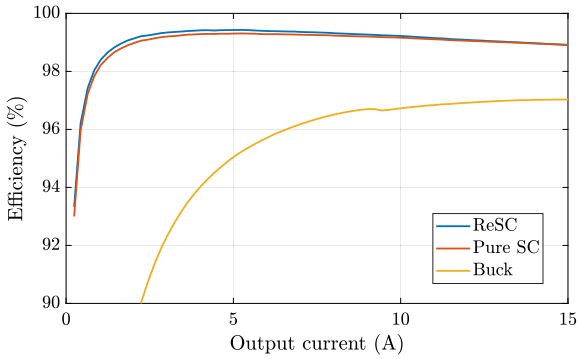

Fig. 9. Measured 48-to-24 V efficiency ($f_{sw} = 100$ kHz).

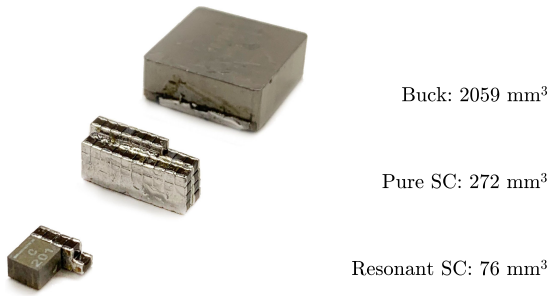

Fig. 10. Required passive component volume to achieve the efficiency performance shown in Fig. 9.

On the other hand, the hardware-based actual volume ratio is $\frac{\text{Vol}_{\text{buck}}}{\text{Vol}_{\text{ReSC}}} = 27$. This is because the selected inductor is oversized with an energy storage capability greater than the required amount. After factoring out the excess stored energy of the inductor $\left(\frac{4\mu H \cdot 30\,A^2}{5.6\mu H \cdot 40\,A^2}\right)$, the true volume ratio $\frac{\text{Vol}_{\text{buck}}}{\text{Vol}_{\text{ReSC}}}$ becomes 11, which closely matches the calculation result. Fig. 10 showcases the required passive component volume of different solutions, and Table III compares the experimental volume ratios with the calculated results. The ReSC converter can deliver its promised benefits and achieve the highest efficiency with significantly less passive component volume than conventional solutions.

IV. GENERALIZED ANALYSIS

So far, we have shown that through reactive power/energy analysis, the total passive component volume of a 2-to-1 ReSC converter can be calculated and optimized based on only P_{out}, f_{sw} (resonant frequency), $\rho_{E,C}$, and $\rho_{E,L}$, by adjusting the capacitor ripple ratio $\frac{\Delta V_{C0}}{V_{C0}}$. There is no need to assume or constrain the L and C values. Next, we generalize this method to arbitrary ReSC topologies with any number of flying capacitors and inductors.

TABLE III
COMPARISON BETWEEN CALCULATION AND EXPERIMENT

	Calculation	Experiment
$\frac{\text{Vol}_{\text{pureSC}}}{\text{Vol}_{\text{ReSC}}}$	4.4	3.6
$\frac{\text{Vol}_{\text{buck}}}{\text{Vol}_{\text{ReSC}}}$	11.5	11*

*After factoring out the excess energy.

A. Equation Formulation

Since all topologies degenerate to the same basic structure at a conversion ratio of 2, we can use the result of the 2-to-1 ReSC converter as a baseline. Assuming the 2-to-1 ReSC converter has inductance L, flying capacitance C, switching frequency $f_{\text{sw}} = \frac{1}{2\pi\sqrt{LC}}$, output voltage V_{out}, and output current I_{out}, its peak-to-peak capacitor voltage ripple can be derived as $\Delta V_{C0} = \frac{I_{\text{out}}}{2Cf_{\text{sw}}}$, and the reactive power rating of the inductor is $P_{L0} = \frac{I_{\text{out}}\Delta V_{C0}}{16}$.

When expanding to higher conversion ratios, the capacitance ratio among the flying capacitors should be first determined by the soft-charging requirement [11] and other practical considerations (e.g., same resonant frequency for different LC tanks). For most common topologies (e.g., series–parallel, Dickson, FCML), all added flying capacitors should have the same capacitance C as compared to the 2-to-1 case. For the Doubler topology [27], the capacitance ratio is $C_1 = C$, $C_2 = \frac{1}{4}C$,..., $C_n = \frac{1}{2^{2n-2}}C$. If an ReSC converter has multiple resonant inductors, it is usually required to have the same resonant frequency for all resonant tanks. Presuming each capacitor has its own resonant tank, then for the topologies with equal capacitance C, all inductors should have the same inductance L. For the Doubler topology, the inductance ratio is $L_1 = L$, $L_2 = 4\,L$,..., $L_n = 2^{2n-2}L$. Additionally, both V_{out} and I_{out} remain the same as in the 2-to-1 case. Now, we can express the reactive power rating $P_{C,i}$, average dc voltage $V_{C,i}$, and ac ripple voltage $\Delta V_{C,i}$ of any given flying capacitor C_i in terms of P_{out}, V_{out}, and ΔV_{C0}

(the capacitor ripple voltage in the 2-to-1 case)

$$C_i \Rightarrow \begin{cases} P_{C,i} = k_i P_{\text{out}} \\ V_{C,i} = \alpha_i V_{\text{out}} \\ \Delta V_{C,i} = \beta_i \Delta V_{C0} \end{cases} \tag{32}$$

where k_i, α_i, and β_i are topology dependent parameters. An example of how these parameters can be derived is given in the next section. Once these parameters are calculated, the ripple voltage ratio of C_i can be expressed as

$$\frac{\Delta V_{C,i}}{V_{C,i}} = \frac{\beta_i \Delta V_{C0}}{\alpha_i V_{\text{out}}} \tag{33}$$

and the energy utilization factor $\mu_{C,i}$ can be generalized from (7) as

$$\mu_{C,i} = \frac{2\frac{\Delta V_{C,i}}{V_{C,i}}}{\left(1+\frac{1}{2}\frac{\Delta V_{C,i}}{V_{C,i}}\right)^2} = \frac{\frac{2\beta_i \Delta V_{C0}}{\alpha_i V_{\text{out}}}}{\left(1+\frac{\beta_i \Delta V_{C0}}{2\alpha_i V_{\text{out}}}\right)^2}. \tag{34}$$

The required energy storage $E_{C_i,\text{store}}$ of capacitor C_i at a switching frequency of f_{sw} can be derived as

$$\begin{aligned} E_{C_i,\text{store}} &= \frac{P_{C,i}}{f_{\text{sw}}\mu_{C,i}} = \frac{k_i P_{\text{out}}}{f_{\text{sw}}\mu_{C,i}} \\ &= \frac{P_{\text{out}}}{f_{\text{sw}}}\left(\frac{k_i}{2} + \frac{k_i\alpha_i}{2\beta_i}\frac{V_{\text{out}}}{\Delta V_{C0}} + \frac{k_i\beta_i}{8\alpha_i}\frac{\Delta V_{C0}}{V_{\text{out}}}\right). \end{aligned} \tag{35}$$

Next, the total required energy storage of the sum of the n flying capacitors is given by

$$\begin{aligned} E_{C,\text{tot}} &= \sum_{i=1}^{n} E_{C_i,\text{store}} \\ &= \frac{P_{\text{out}}}{f_{\text{sw}}}\left(K_{\text{tot}} + A_{\text{tot}}\frac{V_{\text{out}}}{\Delta V_{C0}} + B_{\text{tot}}\frac{\Delta V_{C0}}{V_{\text{out}}}\right) \end{aligned} \tag{36}$$

where $K_{\text{tot}} = \frac{1}{2}\sum_{i=1}^{n} k_i$, $A_{\text{tot}} = \frac{1}{2}\sum_{i=1}^{n}\frac{k_i\alpha_i}{\beta_i}$, and $B_{\text{tot}} = \frac{1}{8}\sum_{i=1}^{n}\frac{k_i\beta_i}{\alpha_i}$. Similarly, the reactive power rating of an inductor L_i can be expressed as a ratio to the P_{L0} in the basic 2-to-1 case

$$P_{L_i} = \gamma_i P_{L0} \tag{37}$$

and the total required energy of the sum of the m inductors is

$$E_{L,\text{tot}} = \sum_{i=1}^{m} E_{L_i} = \frac{P_{L0}}{f_{\text{sw}}}\sum_{i=1}^{m}\gamma_i = \frac{P_{L0}}{f_{\text{sw}}}Y_{\text{tot}} \tag{38}$$

with $Y_{\text{tot}} = \sum_{i=1}^{m}\gamma_i$. Note that this analysis can be applied to different types of ReSC converters with different inductor locations, including "single inductor at output" and "distributed inductors," which are also known as direct- and indirect-conversion in [18] and [25].

Following the same procedure as that shown in (10), we can express the total passive volume as a function of $\frac{\Delta V_{C0}}{V_{\text{out}}}$:

$$\begin{aligned} \text{Vol}_{\text{tot}} = \text{Vol}_{\text{C}} + \text{Vol}_{\text{L}} &= \frac{P_{\text{out}}}{f_{\text{sw}}} \\ &\times \left(\frac{K_{\text{tot}} + A_{\text{tot}}\frac{V_{\text{out}}}{\Delta V_{C0}} + B_{\text{tot}}\frac{\Delta V_{C0}}{V_{\text{out}}}}{\rho_{E,C}} + \frac{\frac{1}{16}Y_{\text{tot}}\frac{\Delta V_{C0}}{V_{\text{out}}}}{\rho_{E,L}}\right). \end{aligned} \tag{39}$$

By differentiating Vol_{tot} with respect to $\frac{\Delta V_{C0}}{V_{\text{out}}}$, the optimized capacitor ripple ratio r^* and the minimized total passive volume $\text{Vol}_{\text{tot,min}}$ can be derived

$$r^* = \left(\frac{\Delta V_{C0}}{V_{\text{out}}}\right)^* = \sqrt{\frac{16A_{\text{tot}}\rho_{E,L}}{16B_{\text{tot}}\rho_{E,L} + Y_{\text{tot}}\rho_{E,C}}} \tag{40}$$

$$\begin{aligned} \text{Vol}_{\text{tot,min}} = \frac{P_{\text{out}}}{f_{\text{sw}}\rho_{E,L}}\Bigg(&\frac{\rho_{E,L}}{\rho_{E,C}}\left(K_{\text{tot}} + A_{\text{tot}}\frac{1}{r^*} + B_{\text{tot}}r^*\right) \\ &+ \frac{Y_{\text{tot}}r^*}{16}\Bigg). \end{aligned} \tag{41}$$

When $\rho_{E,C} \gg \rho_{E,L}$ and $Y_{\text{tot}}\rho_{E,C} \gg 16B_{\text{tot}}\rho_{E,L}$, r^* can be further simplified to

$$r^* = \sqrt{\frac{16A_{\text{tot}}\rho_{E,L}}{16B_{\text{tot}}\rho_{E,L} + Y_{\text{tot}}\rho_{E,C}}} \approx \sqrt{\frac{16A_{\text{tot}}\rho_{E,L}}{Y_{\text{tot}}\rho_{E,C}}} \tag{42}$$

yielding an approximated minimized total volume of

$$\text{Vol}_{\text{tot,min}} \approx \frac{P_{\text{out}}}{f_{\text{sw}}\rho_{E,L}}\left(K_{\text{tot}}\frac{\rho_{E,L}}{\rho_{E,C}} + \frac{1}{2}\sqrt{\frac{A_{\text{tot}}Y_{\text{tot}}\rho_{E,L}}{\rho_{E,C}}}\right). \tag{43}$$

In this expression, no detailed L and C values need to be assumed or constrained. The P_{out}, f_{sw}, $\rho_{E,L}$ and $\rho_{E,C}$ terms depend on the operating condition and the remaining terms are purely topology specific parameters. This equation can be used to quantitatively calculate the minimum achievable passive volume of a large class of hybrid ReSC converters at a given power level and switching frequency. Note that this analysis assumes that all flying capacitors have an energy density of $\rho_{E,C}$ and all resonant inductors have an energy density of $\rho_{E,L}$. For the topologies that use multiple types of capacitors and inductors with different power densities such as [3], (39) can be modified to incorporate multiple ρ_{E,C_i} and ρ_{E,L_i}.

B. Example on N:1 Resonant Series–Parallel Converter

Here, we use an $N:1$ resonant series–parallel converter as an example to demonstrate how the topology dependent parameters α_i, k_i, β_i, and γ_i in (32) and (37) can be derived. As shown in Fig. 11, two types of augmenting inductor(s) can be implemented: distributed inductors and a single inductor at output. Depending on the inductor location, the current waveforms of the inductor(s) and capacitors are different, and the corresponding α_i, k_i, β_i, and γ_i parameters can vary.

1) Calculating α_i: In an $N:1$ series–parallel converter, there are $N-1$ flying capacitors with equal capacitance. All are connected in series in the series-phase ϕ_s and paralleled in the parallel-phase ϕ_p. Through KVL analysis, it can be found that all capacitors have an average dc voltage of V_{out} regardless of the inductor location. According to (32), $V_{C,i} = \alpha_i V_{\text{out}}$, thus

$$\alpha_1 = \alpha_2 = \cdots = \alpha_{N-1} = 1. \tag{44}$$

2) Calculating k_i: As explained in [16], the power processed by a capacitor C_i can be calculated as

$$P_{C,i} = \frac{1}{2}\overline{|\,V_{C,i}I_{C,i}\,|} \tag{45}$$

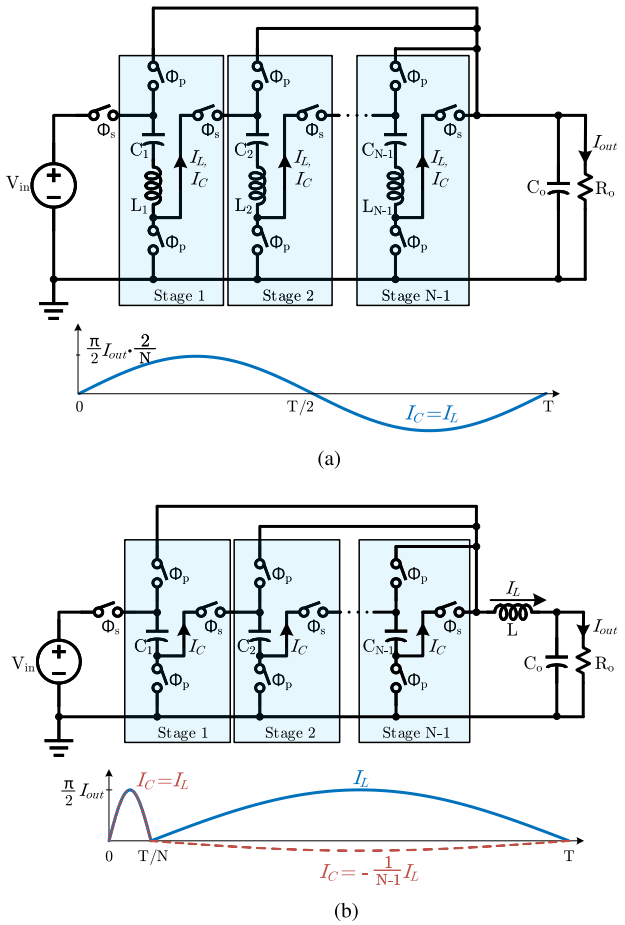

Fig. 11. $N:1$ resonant series–parallel converters with different inductor locations. (a) Distributed inductors. (b) Single inductor at output.

where

$$\overline{|\,V_{C,i}I_{C,i}\,|} \triangleq \frac{1}{T}\int_0^T |\,V_{C,i}(t)I_{C,i}(t)\,|\,dt. \tag{46}$$

The integral term in (46) represents the total energy flowing into and out of the capacitor per switching cycle. For SC-based converters, (45) can be simplified to

$$P_{C,i} = \frac{1}{2}V_{C,i}I_{C,i} \tag{47}$$

where $V_{C,i}$ is the average dc voltage of the flying capacitor and $I_{C,i}$ is the average charging (or discharging) current through C_i. The average charging current is defined as the total charge flowing into the capacitor per switching cycle divided by half of the period

$$I_{C,i} = \frac{Q_{C,i\_in}}{T/2} = \frac{Q_{C,i\_out}}{T/2}. \tag{48}$$

In ReSC converters, the $P_{C,i}$ of a flying capacitor is irrespective to the location of the augmenting inductor(s), and is the same as that in its pure SC counterpart. As illustrated in Fig. 11(a), with *distributed inductors*, the $N:1$ series–parallel converter has a 50% duty ratio for both phases. Thus, the average capacitor charging current is the average value of the half sine-wave: $I_{C,i} = \frac{2}{N}I_{\text{out}}$.

With *a single inductor at output*, the duration and peak amplitude of the sinusoidal capacitor charging current become $\frac{T}{N}$ and $\frac{\pi}{2}I_{\text{out}}$, respectively. By applying (48), it can be found that the average capacitor charging current is the same as that with distributed inductors: $I_{C,i} = \frac{I_{\text{out}}\cdot\frac{T}{N}}{T/2} = \frac{2}{N}I_{\text{out}}$.

With $I_{C,i} = \frac{2}{N}I_{\text{out}}$ and $V_{C,i} = V_{\text{out}}$, we get $P_{C,i} = \frac{1}{2}V_{C,i}I_{C,i} = \frac{1}{N}V_{\text{out}}I_{\text{out}}$. In (32), k_i is defined as $P_{C,i} = k_i V_{\text{out}}I_{\text{out}}$, therefore

$$k_1 = k_2 = \cdots = k_{N-1} = \frac{1}{N}. \tag{49}$$

3) Calculating β_i: The voltage on capacitor C_i is $V_{C,i} - \frac{I_{pk_{c,i}}}{C_i\omega_{r_{c,i}}}cos(\omega_{r_{c,i}}t)$. Thus, its peak-to-peak voltage ripple is

$$\Delta V_{C,i} = \frac{2I_{pk_{c,i}}}{C_i\omega_{r_{c,i}}} \tag{50}$$

where $I_{pk_{c,i}}$ is the peak current flowing through C_i and $\omega_{r_{c,i}}$ is the frequency of the resonant tank C_i is in.

For the *distributed inductor* configuration in Fig. 11(a), each C_i formulates a resonant tank with a series-connected inductor L_i. As discussed in Section IV-A, C_i and L_i should be equal to the baseline value C and L in the basic 2-to-1 case. Therefore, $\omega_{r_{c,i}}$ is the also the same as that in the 2-to-1 case, whereas the peak current $I_{pk_{c,i}}$ is $\frac{2}{N}$ times of the baseline value I_{pk}, yielding $\Delta V_{C,i} = \frac{2}{N}\Delta V_{C0}$ and

$$\beta_{1,dis} = \beta_{2,dis} = \cdots = \beta_{N-1,dis} = \frac{2}{N}. \tag{51}$$

For the *single inductor at output* configuration in Fig. 11(b), the duty ratio of ϕ_s changes to $\frac{T}{N}$ to maintain capacitor charge balance. In ϕ_s, all capacitors are connected in series ($C_{\text{eq}} = \frac{1}{N-1}C$) and the charging current is equal to the output current: $I_{pk} = \frac{\pi}{2}I_{\text{out}}$. The voltage ripple of each capacitor is

$$\Delta V_{C,i} = \frac{1}{N-1}\cdot\frac{2I_{pk}}{C_{\text{eq}}\frac{1}{\sqrt{LC_{\text{eq}}}}} = \frac{1}{\sqrt{N-1}}\Delta V_{C0} \tag{52}$$

leading to a different set of β values compared to the distributed inductor case

$$\beta_{1,\text{single}} = \beta_{2,\text{single}} = \cdots = \beta_{N-1,\text{single}} = \frac{1}{\sqrt{N-1}}. \tag{53}$$

4) Calculating γ_i: The reactive power rating of an inductor L_i can be calculated with the integral method described in (4). Alternatively, since L_i should be equal to the baseline value L in the 2-to-1 case, the calculation can be simplified by relating $P_{L,i}$ to P_{L0} directly. Two parameters need to be compared to the baseline values in the 2-to-1 case: the amplitude of the peak inductor current $I_{pk_{L,i}}$ and the effective switching period T_{eff}.

For the *distributed inductor* case, the inductor current is related to the baseline current by $I_{pk_{L,i}} = \frac{2}{N}I_{pk}$, resulting in $E_{L,i} = \frac{4}{N^2}E_{L0}$. Since $T_{\text{eff}} = T = 2\pi\sqrt{LC}$ is the same as that in the 2-to-1 case, $P_{L,i} = \frac{E_{L,i}}{T_{\text{eff}}} = \frac{4}{N^2}P_{L0}$ and

$$\gamma_{1,dis} = \gamma_{2,dis} = \cdots = \gamma_{N-1,dis} = \frac{4}{N^2}. \tag{54}$$

TABLE IV
KEY PARAMETERS OF $N:1$ SERIES–PARALLEL CONVERTER

	k_i	α_i	β_i	γ_i
Distributed inductors	$\frac{1}{N}$	1	$\frac{2}{N}$	$\frac{4}{N^2}$
Single inductor	$\frac{1}{N}$	1	$\frac{1}{\sqrt{N-1}}$	$\frac{2\sqrt{N-1}}{N}$

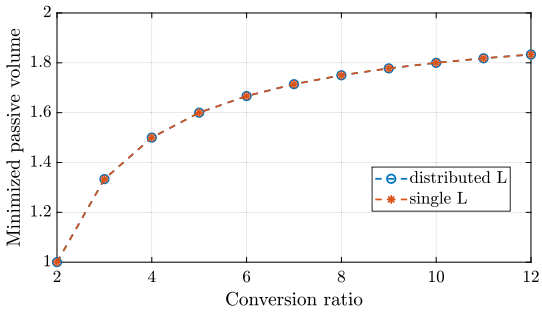

Fig. 12. Minimized total passive volume of $N:1$ resonant series–parallel converters with different inductor locations (normalized to the 2-to-1 case).

For the *single inductor at output* case, the inductor sees the entire output current $I_{pk_{L,i}} = I_{pk}$ and therefore $E_{L,i} = E_{L0}$. The effective switching period can be calculated as the average of the series resonant period and the parallel resonant period

$$\begin{aligned} T_{\text{eff}} &= \frac{T_{\text{series}} + T_{\text{parallel}}}{2} \\ &= \frac{2\pi\left(\sqrt{L\frac{C}{N-1}} + \sqrt{L(N-1)C}\right)}{2} \\ &= 2\pi\sqrt{LC}\cdot\frac{N}{2\sqrt{N-1}} \end{aligned} \tag{55}$$

resulting in $P_{L,i} = \frac{2\sqrt{N-1}}{N}P_{L0}$ and

$$\gamma_{\text{single}} = \frac{2\sqrt{N-1}}{N}. \tag{56}$$

The calculated topology dependent parameters are summarized in Table IV. It can be seen that the capacitor ripple term β_i and the inductor power term γ_i are different for the two types of inductor location. Nevertheless, as shown in Fig. 12, they can achieve the same minimized total passive volume, as calculated from (41). This example demonstrates that the proposed method can work for generalized ReSC topologies with different inductor placement strategies.

While this analysis shows similar performance for single versus distributed inductor version of the series–parallel converter, in practice there may be a penalty for using multiple small inductors compared to one large inductor. This is because the fundamental scaling law dictates that the achievable energy density scales with size and magnetic components perform worse at small size [28]. Besides energy density consideration, a single large inductor is also preferred from loss perspective. Using power spectral density (PSD) analysis, McLaughlin *et al.* [18], Kesarwani and Stauth [29] demonstrated that the single inductor at output configuration (also known as direct-conversion) has lower inductor losses as the majority of the power is concentrated at dc, whereas the distributed inductor case (indirect-conversion) has higher size-normalized losses due to the fact that its PSD is concentrated at harmonics of the switching frequency with no dc component.

V. RESC TOPOLOGY COMPARISON

Besides optimizing the total passive component volume, the proposed method can also be used to compare the relative volume of different ReSC topologies. In order to compare the efficacy of passive component utilization of different topologies, the amount of energy transferred by each topology should be kept the same, i.e., $E_{\text{out}} = \frac{P_{\text{out}}}{f_{\text{sw}}}$ is fixed. Alternatively speaking, it is of interest to calculate and compare the passive component volume required by each topology at a desired P_{out} and f_{sw}. This volume can be normalized to become a passive component utilization factor, whose implication is similar to that of switch VA rating for practical deisgns—A topology with better passive component utilization either can operate at a lower switching frequency given the same passive component volume, resulting in lower power loss; or can operate at the same switching frequency with smaller passive volume, therefore, achieving higher power density.

It can be observed from (43) that the expression of the minimized total passive volume of ReSC converters consists of two parts. The first part $\frac{P_{\text{out}}}{f_{\text{sw}}\rho_{E,L}}$ depends on the operating condition, and can be viewed as the volume of an inductor that stores all of the energy delivered to the load in each switching cycle. The remaining part contains topology dependent parameters and the energy density ratio of capacitor and inductor. It represents the relative volume ratio to an inductor whose volume is $\frac{P_{\text{out}}}{f_{\text{sw}}\rho_{E,L}}$ and can be viewed as a "passive component utilization factor" of the topology. By normalizing (43) to $\frac{P_{\text{out}}}{f_{\text{sw}}\rho_{E,L}}$, a normalized passive component volume M_p is defined as

$$\begin{aligned} M_p &= \frac{\text{Vol}_{\text{tot,min}}}{\frac{P_{\text{out}}}{f_{\text{sw}}\rho_{E,L}}} \\ &= \frac{\rho_{E,L}}{\rho_{E,C}}\left(K_{\text{tot}} + A_{\text{tot}}\frac{1}{r^*} + B_{\text{tot}}r^*\right) + Y_{\text{tot}}r^* \end{aligned} \tag{57}$$

which is independent of f_{sw} and P_{out}. It reflects the intrinsic passive component utilization capability of a topology and can be used for direct comparison among different topologies.

Here, we compare the normalized passive component volume M_p of various ReSC topologies that are adapted from common SC converters [3], [25], [30]–[32]. The circuit schematic of the series–parallel topology is shown in Fig. 11 and the schematics of the other topologies under investigation are shown in Fig. 13. Their M_p values are calculated and plotted in Fig. 14, and a buck converter is included for reference. Even though empirical data shows that the ratio of $\frac{\rho_{E,C}}{\rho_{E,L}}$ can be as high as 1000 [33], a relatively conservative ratio of $\frac{\rho_{E,C}}{\rho_{E,L}} = 100$ is used in this comparison. The buck converter is assumed to operate at the boundary conduction mode such that its inductor energy utilization is maximized.

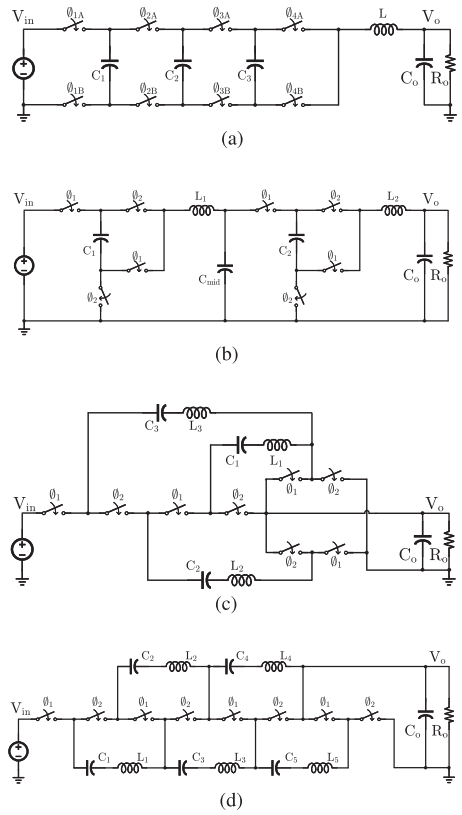

Fig. 13. Schematic drawing of various 4-to-1 ReSC converter topologies. (a) FCML. (b) Doubler. (c) Dickson. (d) Ladder.

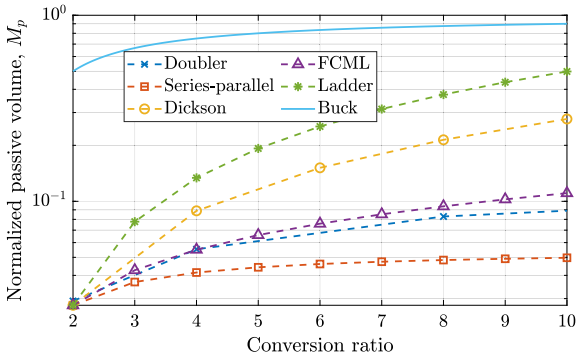

Fig. 14. Normalized passive volume (assuming $\rho_{E,C}/\rho_{E,L} = 100$). Lower is better.

It can be seen from Fig. 14 that, thanks to the high energy density of capacitors, all ReSC converters outperform the buck converter by a wide margin, especially at relatively low conversion ratios. In particular, the series–parallel topology achieves the lowest passive component volume among all topologies. This result agrees with the finding in [20] and [33], where the series–parallel converter is at the theoretical Wolaver limit [16] of passive components. Additionally, although requiring high voltage capacitors, the FCML topology achieves relatively good passive component utilization, owing to the frequency multiplication effect that reduces the energy storage requirement of the components.

For the same switching frequency, a lower total switch stress indicates a potentially lower conduction loss, lower switching

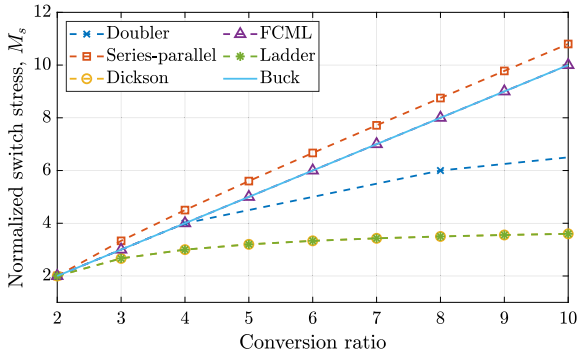

Fig. 15. Normalized switch stress. Lower is better.

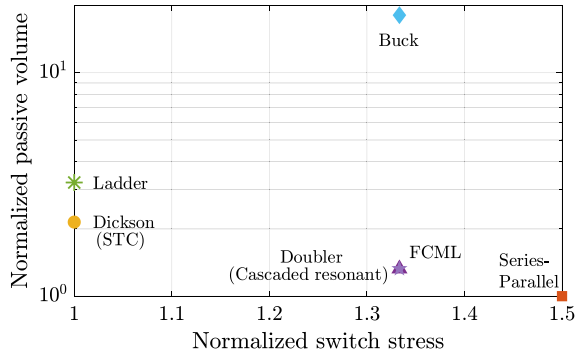

Fig. 16. 4-to-1 ReSC topology comparison.

loss, and smaller switch size. Therefore, it can be used as a good indication of potential efficiency [34]. The switch stress is defined as

$$\text{Total switch stress} = \sum_{\text{switches}} V_{\text{ds}} I_{\text{ds}} \tag{58}$$

where V_{ds} is the peak blocking voltage seen by the switch and I_{ds} is the average current through the switch. Note that even though the RMS current value should be used for the best accuracy when the duty ratio deviates from 50% [35], [36] has shown that the effect of RMS/dc ratio on the total switch stress is relatively mild. Therefore, the average current value is used here as a close approximation. Since one can express V_{ds} using the output voltage ($\beta_v V_{\text{out}}$), and I_{ds} using the output current ($\beta_i I_{\text{out}}$), the normalized switch stress M_s can be defined as

$$M_s = \frac{\sum_{\text{switches}} V_{ds} I_{ds}}{V_{\text{out}} I_{\text{out}}} = \sum_{\text{switches}} \beta_v \beta_i. \tag{59}$$

This can be viewed as the total switch power rating necessary to deliver a certain power to the output. More details regarding this metric can be found in [37]. Fig. 15 shows the calculated M_s of the topologies of interest, with the Dickson [38], [39] and Ladder topologies at the Wolaver limit [20]. It should be emphasized that the derived M_p and M_s reflect the intrinsic performance of passive and active component utilization and are independent of detailed operating conditions (e.g., P_{out}, f_{sw}).

Fig. 16 compares the relative performance of various topologies at a ratio of 4:1. In general, the topologies that have high normalized switch stress tend to have lower normalized passive volume, and vice versa. With the series–parallel and Dickson topologies at the theoretical boundaries of passive and active

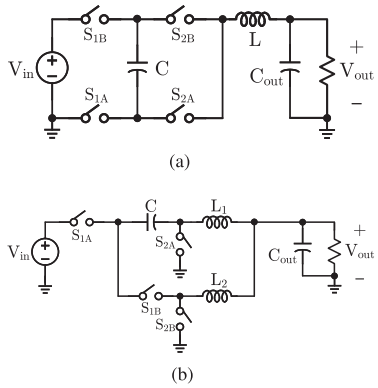

Fig. 17. Schematic drawings of two example regulated hybrid converters. (a) 3-level buck converter. (b) Series-capacitor buck converter.

component Wolaver limits, respectively, all other classical and emerging topologies will fit inside those bounds. Note that the switched-tank converter (STC) [3] has the same theoretical performance as the Dickson as they share the same fundamental structure. This plot allows designers to quickly visualize and compare the tradeoffs of different solutions.

It should be noted that practical converter designs have more considerations and the actual performance of different topologies can be different than what is plotted here. For instance, the lowest voltage rating of widely available discrete power MOSFETS is at present about 25 V. Thus, for discrete applications with input voltage lower than 25 V, the topologies with low switch voltage rating and switch VA stress (e.g., Dickson) cannot fully utilize their potential. In this case, the topology efficiency comparison should be based on switch conductance G rather than GV^2 (VA rating) [35]. Then, it is found that the series–parallel topology can achieve one of the lowest output impedances among all ReSC topologies, even though its normalized switch stress is the highest in Fig. 16. In addition, the implementation complexity should also be considered, such as the number of components, the design of gate drive circuit, and the ease of PCB layout. This may put the doubler topology in an attractive position because of its simple and highly modular design.

VI. Comparison of Regulated Hybrid Converters

So far, all analysis has focused on fixed-ratio ReSC converters, in which the inductors see only the flying capacitor voltage ripples. Next, we briefly discuss how the reactive energy/power calculation can be applied to analyze and compare hybrid SC converters with regulation capability. In such converters, the SC stage is typically combined with a buck stage. The buck converter stage can achieve voltage regulation through pulsewidth modulation (PWM), while serving as a current source for capacitor soft-charging operation.

Here, we analyze two basic hybrid converter topologies, the three-level buck converter and the series-capacitor buck converter. Their circuit schematics are shown in Fig. 17. In spite of having of the same number of switches and flying capacitor, they have very different operating characteristics and advantages owing to different inductor placement strategies. Fig. 18 plots

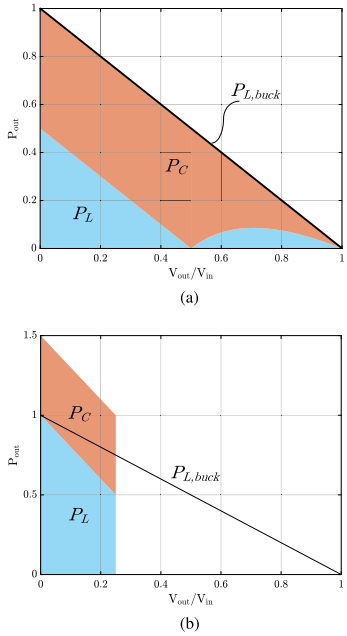

Fig. 18. Average power processed by the passive components in hybrid converters. (a) 3-level buck converter. (b) Series-capacitor buck converter.

the reactive power rating of the passive components of the two converters as a function of the conversion ratio $\frac{V_{\text{out}}}{V_{\text{in}}}$. The detailed calculation for the three-level buck converter is provided in the Appendix as an example.

This reactive power analysis can directly reflect the passive component utilization of a hybrid converter. In [16], Wolaver derived that the reactive power P_{ind} that needs to be processed by a converter with a gain of G ($G = \frac{V_{\text{in}}}{V_{\text{out}}}$ for a step-down converter) is governed by $P_{\text{ind}} \geq \frac{G-1}{G} P_{\text{out}}$. It can be seen from Fig. 18(a) that the total reactive power of the three-level buck converter is equal to that of a conventional buck converter, which is known to be at the Wolaver limit. Thanks to the reduced voltage stress and the frequency doubling effect, the inductor experiences less volt–second and processes significantly less power than a conventional buck converter. Even though the total processed power remains the same, a great portion is now processed by the high energy-density flying capacitor, resulting in reduced total passive component volume and less power loss on the inductor. When $\frac{V_{\text{out}}}{V_{\text{in}}} = 0.5$, there is no voltage across the inductor except for the flying capacitor voltage ripple. Therefore, the 2-to-1 ReSC converter can be viewed as a special case of three-level buck converter with minimum required inductance, at the cost of no regulation capability.

The series-capacitor buck converter can be viewed as a 2-to-1 SC converter cascaded by a two-phase interleaved buck converter, whose maximum duty ratio is 0.5. This leads to a maximum conversion ratio of $\frac{V_{\text{out}}}{V_{\text{in}}} = 0.25$. Its detailed operating principle can be found in [40]–[42]. The reactive power processed by the series-capacitor buck converter is shown in Fig. 18(b). Because of the nature of cascaded converters, its total processed reactive power is unavoidably higher than the Wolaver limit. However, the series-capacitor buck still has the potential to achieve lower total passive component volume and higher power density than the conventional buck converter. It can be shown

that the power processed by the flying capacitor is a fixed value of $P_C = \frac{1}{2}P_{\text{out}}$, whereas the inductor power is equal to that of a buck converter with half of the input voltage $P_L = \frac{G-2}{G}P_{\text{out}}$. When $\frac{V_{\text{out}}}{V_{\text{in}}} = 0.25$, the power processed by the inductor is 33% lower than that of a buck converter rated for the full input voltage. Even for a high conversion ratio of $\frac{V_{\text{out}}}{V_{\text{in}}} = 0.1$, an 11% inductor power rating reduction is achieved. Given the same switching frequency and inductance value, this can be translated to an 11% inductor current ripple reduction. This property is noteworthy since even meager reductions in inductor current ripple may result in significant savings in inductor power loss. Additionally, the series-capacitor buck converter has attractive features such as reduced switching loss owing to lower voltage stress on switches, and automatic current balancing for interleaving operation.

To calculate and compare the total passive component volume of different topologies at a given conversion ratio, a current ripple ratio of the inductor and a voltage ripple ratio of the flying capacitor need to be determined first. Then, the corresponding energy utilization factors and the passive component volume can be derived with the method presented in Section II. Considered the very high energy density ratio between capacitor and inductor (e.g., $\frac{\rho_{E,C}}{\rho_{E,L}} > 100$), it is desirable to use the SC network to achieve the majority of the required voltage conversion, so that the voltage and power stress of the following buck stage can be reduced. This strategy has the potential to further reduce both the total passive component volume and the power loss on the inductor, if the implementation complexity of the SC stage can be properly managed. Recently, an improved series-capacitor buck converter with an 8-to-1 SC stage is presented in [43].

VII. Conclusion

This article models the passive component volume of hybrid resonant SC converters from the perspective of the reactive energy/power processed by the passive components. It is shown that the total passive component volume can be expressed as a function of flying capacitor voltage ripple ratio, and the optimum inductor and capacitor allocation that minimizes the total volume is dependent on their relative energy density and topology specific parameters. Detailed analysis and experimental results are also provided to showcase that a 2-to-1 ReSC converter can use significantly less passive volume than conventional SC and buck converters for the same power conversion, while maintaining the best efficiency performance. To compare the passive component utilization of different ReSC topologies, a normalized passive volume parameter is proposed for direct and fair comparison. Along with the normalized switch stress parameter (based on switch VA ratings), a framework to compare the relative performances of ReSC topologies is created. Using the proposed method, the series–parallel topology exists at the theoretical lower limit of passive volume, whereas the Dickson and the Ladder topologies exist at the lower limit of switch stress. These boundaries can ultimately help evaluate the performance of other newly proposed topologies. Last, the proposed passive component modeling method is extended to analyze and compare hybrid SC converters with regulation capabilities.

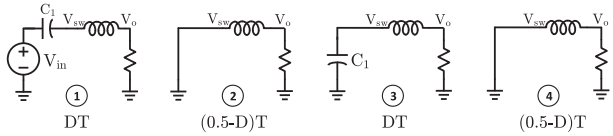

Fig. 19. Circuit operating states at $D < 0.5$.

Appendix

Here, we detail the reactive power calculation of a three-level buck converter. Its schematic drawing is shown in Fig. 17(a). Since the circuit operating states are different for duty ratio $D < 0.5$ and $D > 0.5$, the calculations are carried out for these two intervals separately.

A. $D < 0.5$

The four circuit operating states and the corresponding durations are shown in Fig. 19. Assuming the flying capacitor C_1 is at its nominal voltage $\frac{1}{2}V_{\text{in}}$ with no voltage ripple, then the switch node voltage V_{sw} will be at $\frac{1}{2}V_{\text{in}}$ during state 1 and 3, and at ground during state 2 and 4. Since C_1 is only charged in one state (state 1) and discharged in another (state 3), its processed power equals the charging power at state 1 (or the discharging power at state 3). Assuming the inductor current is constant, we find

$$\begin{aligned} P_C &= P_{C,\text{state1}} \\ &= \frac{\frac{1}{2}V_{\text{in}}I_{\text{out}}DT}{T} \\ &= \frac{1}{2}\frac{V_{\text{out}}}{D}I_{\text{out}}D \\ &= \frac{1}{2}P_{\text{out}}. \end{aligned} \tag{60}$$

It can be seen that the power processed by the flying capacitor is a constant for $D < 0.5$.

The power processed by the inductor can be calculated in a similar way. However, since it transfers energy twice per switching cycle, only one charging state should be considered for reactive power rating calculation

$$\begin{aligned} P_L &= P_{L,\text{state1}} \\ &= \left(\frac{1}{2}V_{\text{in}} - V_{\text{out}}\right)I_{\text{out}}D \\ &= \left(\frac{1}{2} - D\right)\frac{V_{\text{out}}}{D}I_{\text{out}}D \\ &= \left(\frac{1}{2} - D\right)P_{\text{out}}. \end{aligned} \tag{61}$$

B. $D > 0.5$

The circuit operating states for $D > 0.5$ are shown in Fig. 20, and the capacitor and inductor power can be calculated as follows:

$$\begin{aligned} P_C &= P_{C,\text{state2}} \\ &= \frac{1}{2}V_{\text{in}}I_{\text{out}}(1-D) \end{aligned}$$

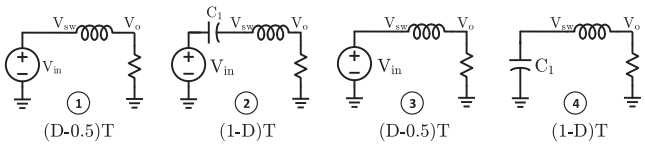

Fig. 20. Circuit operating states at $D > 0.5$.

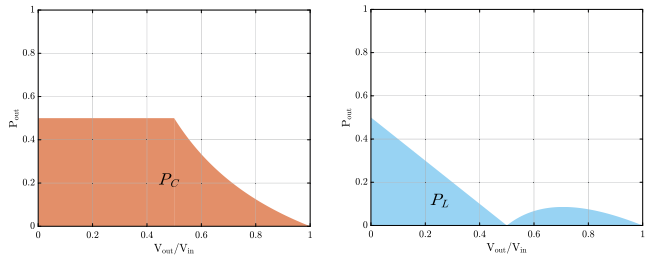

Fig. 21. Reactive power processed by the passive components of a three-level buck converter. (a) Capacitor power. (b) Inductor power.

$$= \frac{1-D}{2D} P_{\text{out}} \tag{62}$$

$$\begin{aligned} P_L &= P_{L,\text{state1}} \\ &= (V_{\text{in}} - V_{\text{out}}) I_{\text{out}} (D - 0.5) \\ &= (1-D) \frac{V_{\text{out}}}{D} I_{\text{out}} (D - 0.5) \\ &= \left(-D + \frac{3}{2} - \frac{1}{2D} \right) P_{\text{out}}. \end{aligned} \tag{63}$$

The above calculated P_C and P_L are plotted in Fig. 21, and the combined total reactive power is plotted in Fig. 18(a).

REFERENCES

[1] Z. Ye, Y. Lei, and R. C. N. Pilawa-Podgurski, "The cascaded resonant converter: A hybrid switched-capacitor topology with high power density and efficiency," *IEEE Trans. Power Electron.*, vol. 35, no. 5, pp. 4946–4958, May 2020.

[2] P. H. McLaughlin, P. A. Kyaw, M. H. Kiani, C. R. Sullivan, and J. T. Stauth, "Two-phase interleaved resonant switched-capacitor DC-DC converter with coupled inductors and custom LC resonator," in *Proc. IEEE Appl. Power Electron. Conf. Expo.*, 2019, pp. 37–44.

[3] S. Jiang, S. Saggini, C. Nan, X. Li, C. Chung, and M. Yazdani, "Switched tank converters," *IEEE Trans. Power Electron.*, vol. 34, no. 6, pp. 5048–5062, Jun. 2019.

[4] Y. Li, X. Lyu, D. Cao, S. Jiang, and C. Nan, "A 98.55% efficiency switched-tank converter for data center application," *IEEE Trans. Ind. Appl.*, vol. 54, no. 6, pp. 6205–6222, Nov./Dec. 2018.

[5] M. Halamicek, T. McRae, N. Vukadinović, and A. Prodić, "Modulation scheme for an effective increase in the number of levels of DC-DC multi-level flying capacitor converters," in *Proc. IEEE Appl. Power Electron. Conf. Expo.*, 2019, pp. 45–49.

[6] R. Das, G. Seo, and H. Le, "Analysis of dual-inductor hybrid converters for extreme conversion ratios," *IEEE Trans. Emerg. Sel. Topics Power Electron.*, vol. 9, no. 5, pp. 5249–5260, Oct. 2021.

[7] C. Li and J. A. Cobos, "A switched capacitor and autotransformer hybrid converter with dc current in the windings," *IEEE Trans. Power Electron.*, vol. 37, no. 2, pp. 1870–1884, Feb. 2022.

[8] R. C. N. Pilawa-Podgurski, D. M. Giuliano, and D. J. Perreault, "Merged two-stage power converter architecture with softcharging switched-capacitor energy transfer," in *Proc. IEEE Power Electron. Specialists Conf.*, 2008, pp. 4008–4015.

[9] R. C. N. Pilawa-Podgurski and D. J. Perreault, "Merged two-stage power converter with soft charging switched-capacitor stage in 180 nm CMOS," *IEEE J. Solid-State Circuits*, vol. 47, no. 7, pp. 1557–1567, Jul. 2012.

[10] R. C. N. Pilawa-Podgurski, "Architectures and circuits for low-voltage energy conversion and applications in renewable energy and power management," Ph.D. dissertation, MIT Press, Cambridge, MA, USA, 2012. [Online]. Available: https://dspace.mit.edu/handle/1721.1/71485

[11] Y. Lei and R. C. N. Pilawa-Podgurski, "A general method for analyzing resonant and soft-charging operation of switched-capacitor converters," *IEEE Trans. Power Electron.*, vol. 30, no. 10, pp. 5650–5664, Oct. 2015.

[12] Y. Lei, W.-C. Liu, and R. C. N. Pilawa-Podgurski, "An analytical method to evaluate and design hybrid switched-capacitor and multilevel converters," *IEEE Trans. Power Electron.*, vol. 33, no. 3, pp. 2227–2240, Mar. 2018.

[13] Z. Ye, S. R. Sanders, and R. C. N. Pilawa-Podgurski, "Modeling and comparison of passive component volume of hybrid resonant switched-capacitor converters," in *Proc. 20th Workshop Control Model. Power Electron.*, 2019, pp. 1–8.

[14] J. A. Cobos, H. Cristóbal, D. Serrano, R. Ramos, J. A. Oliver, and P. Alou, "Differential power as a metric to optimize power converters and architectures," in *Proc. IEEE Energy Convers. Congr. Expo.*, 2017, pp. 2168–2175.

[15] C. Li, D. Serrano, and J. A. Cobos, "A comparative study of hybrid dc-dc converters by indirect power," in *Proc. IEEE Appl. Power Electron. Conf. Expo.*, 2021, pp. 1294–1301.

[16] D. H. Wolaver, "Fundamental study of DC to DC conversion systems," Ph.D. dissertation, MIT Press, Cambridge, MA, USA, 1969.

[17] S. Coday, C. B. Barth, and R. C. N. Pilawa-Podgurski, "Characterization and modeling of ceramic capacitor losses under large signal operating conditions," in *Proc. IEEE 19th Workshop Control Model. Power Electron.*, 2018, pp. 1–8.

[18] P. H. McLaughlin, J. S. Rentmeister, M. H. Kiani, and J. T. Stauth, "Analysis and comparison of hybrid-resonant switched-capacitor DC-DC converters with passive component size constraints," *IEEE Trans. Power Electron.*, vol. 36, no. 3, pp. 3111–3125, Mar. 2021.

[19] M. H. Kiani and J. T. Stauth, "Passive component modeling and optimal size allocation for hybrid-resonant switched capacitor DC-DC converters," in *Proc. IEEE 19th Workshop Control Model. Power Electron.*, 2018, pp. 1–8.

[20] M. D. Seeman, "A design methodology for switched-capacitor dc-dc converters," Ph.D. dissertation, Univ. California, Berkeley, CA, USA, 2009.

[21] G. Schrom, P. Hazucha, F. Paillet, D. Gardner, S. Moon, and T. Karnik, "Optimal design of monolithic integrated DC-DC converters," in *Proc. IEEE Int. Conf. Des. Technol.*, 2006, pp. 1–3.

[22] M. D. Seeman and S. R. Sanders, "Analysis and optimization of switched-capacitor DC-DC converters," *IEEE Trans. Power Electron.*, vol. 23, no. 2, pp. 841–851, Mar. 2008.

[23] S. Pasternak, C. Schaef, and J. Stauth, "Equivalent resistance approach to optimization, analysis and comparison of hybrid/resonant switched-capacitor converters," in *Proc. IEEE 17th Workshop Control Model. Power Electron.*, 2016, pp. 1–8.

[24] H. P. Le, S. R. Sanders, and E. Alon, "Design techniques for fully integrated switched-capacitor DC-DC converters," *IEEE J. Solid-State Circuits*, vol. 46, no. 9, pp. 2120–2131, Sep. 2011.

[25] C. Schaef, J. S. Rentmeister, and J. Stauth, "Multimode operation of resonant and hybrid switched-capacitor topologies," *IEEE Trans. Power Electron.*, vol. 33, no. 12, pp. 10512–10523, Dec. 2018.

[26] Y. Zhu, Z. Ye, and R. C. N. Pilawa-Podgurski, "Modeling and analysis of switched-capacitor converters with finite terminal capacitances," in *Proc. IEEE Appl. Power Electron. Conf. Expo.*, 2021, pp. 178–185.

[27] Z. Ye, Y. Lei, and R. C. N. Pilawa-Podgurski, "A 48-to-12 V cascaded resonant switched-capacitor converter for data centers with 99% peak efficiency and 2500 W/in3 power density," in *Proc. IEEE Appl. Power Electron. Conf. Expo.*, 2019, pp. 13–18.

[28] C. R. Sullivan, B. A. Reese, A. L. F. Stein, and P. A. Kyaw, "On size and magnetics: Why small efficient power inductors are rare," in *Proc. Int. Symp. 3D Power Electron. Integration Manuf.*, 2016, pp. 1–23.

[29] K. Kesarwani and J. T. Stauth, "The direct-conversion resonant switched capacitor architecture with merged multiphase interleaving: Cost and performance comparison," in *Proc. IEEE Appl. Power Electron. Conf. Expo.*, 2015, pp. 952–959.

[30] Z. Ye, Y. Lei, and R. C. N. Pilawa-Podgurski, "A resonant switched capacitor based 4-to-1 bus converter achieving 2180 W/in3 power density and 98.9% peak efficiency," in *Proc. IEEE Appl. Power Electron. Conf. Expo.*, 2018, pp. 121–126.

[31] J. T. Stauth, M. D. Seeman, and K. Kesarwani, "A resonant switched-capacitor IC and embedded system for sub-module photovoltaic power management," *IEEE J. Solid-State Circuits*, vol. 47, no. 12, pp. 3043–3054, Dec. 2012.
[32] C. Schaef and J. T. Stauth, "A highly integrated series-parallel switched-capacitor converter with 12 V input and quasi-resonant voltage-mode regulation," *IEEE Trans. Emerg. Sel. Topics Power Electron.*, vol. 6, no. 2, pp. 456–464, Jun. 2018.
[33] S. R. Sanders, E. Alon, H. Le, M. D. Seeman, M. John, and V. W. Ng, "The road to fully integrated DC-DC conversion via the switched-capacitor approach," *IEEE Trans. Power Electron.*, vol. 28, no. 9, pp. 4146–4155, Sep. 2013.
[34] S. R. Pasternak, M. H. Kiani, J. S. Rentmeister, and J. T. Stauth, "Modeling and performance limits of switched-capacitor DC-DC converters capable of resonant operation with a single inductor," *IEEE Trans. Emerg. Sel. Topics Power Electron.*, vol. 5, no. 4, pp. 1746–1760, Dec. 2017.
[35] W. C. Liu, Z. Ye, and R. C. N. Pilawa-Podgurski, "Comparative analysis on minimum output impedance of fixed-ratio hybrid switched capacitor converters," in *Proc. IEEE 20th Workshop Control Model. Power Electron.*, 2019, pp. 1–6.
[36] M. H. Kiani and J. T. Stauth, "Optimization and comparison of hybrid-resonant switched capacitor DC-DC converter topologies," in *Proc. IEEE 18th Workshop Control Model. Power Electron.*, 2017, pp. 1–8.
[37] Y. Lei, "High-performance power converters leveraging capacitor-based energy transfer," Ph.D. dissertation, Univ. Illinois, Urbana, IL, USA, 2017. [Online]. Available: http://hdl.handle.net/2142/97413
[38] Y. Lei, R. May, and R. Pilawa-Podgurski, "Split-phase control: Achieving complete soft-charging operation of a Dickson switched-capacitor converter," *IEEE Trans. Power Electron.*, vol. 31, no. 1, pp. 770–782, Jan. 2016.
[39] Y. Lei, Z. Ye, and R. C. N. Pilawa-Podgurski, "A GAN-based 97% efficient hybrid switched-capacitor converter with lossless regulation capability," in *Proc. IEEE Energy Convers. Congr. Expo.*, 2015, pp. 4264–4270.
[40] K. Nishijima, K. Harada, T. Nakano, T. Nabeshima, and T. Sato, "Analysis of double step-down two-phase buck converter for VRM," in *Proc. 27th Int. Telecommun. Conf.*, 2005, pp. 497–502.
[41] K. Abe, K. Nishijima, K. Harada, T. Nakano, T. Nabeshima, and T. Sato, "A novel three-phase buck converter with bootstrap driver circuit," in *Proc. IEEE Power Electron. Specialists Conf.*, 2007, pp. 1864–1871.
[42] P. S. Shenoy, M. Amaro, J. Morroni, and D. Freeman, "Comparison of a buck converter and a series capacitor buck converter for high-frequency, high-conversion-ratio voltage regulators," *IEEE Trans. Power Electron.*, vol. 31, no. 10, pp. 7006–7015, Oct. 2016.
[43] Z. Ye, R. A. Abramson, Y. L. Syu, and R. C. N. Pilawa-Podgurski, "MLB-POL: A high performance hybrid converter for direct 48 V to point-of-load applications," in *Proc. IEEE 21st Workshop Control Model. Power Electron.*, 2020, pp. 1–8.

Zichao Ye (Graduate Student Member, IEEE) received the B.S. (with highest hons.) and M.S. degrees from the University of Illinois at Urbana-Champaign, Champaign, IL, USA, in 2014 and 2016, respectively, and the Ph.D. degree from the University of California Berkeley, Berkeley, CA, USA, in 2020, all in electrical engineering.

His prior works include switched capacitor topology modeling and comparison, compact and efficient floating gate drive power supply design, flying capacitor voltage balancing and efficient data center power delivery. He has coauthored more than 30 journals and conference publications. His research interests include high density and high efficiency power converter design, with specific interests in hybrid and resonant switched capacitor converters and flying capacitor multilevel converters.

Dr. Ye was the recipient of the IEEE Workshop on Control and Modeling of Power Electronics Best Paper Award, in 2017, IEEE Applied Power Electronics Conference Best Presentation Award, in 2019, and IEEE Power Electronics Society Ph.D. Thesis Talk Award, in 2021. He was also the recipient of the 2021 David J. Sakrison Memorial Award from the Electrical Engineering and Computer Sciences Department of the University of California Berkeley for completing a truly outstanding piece of dissertation research.

Seth R. Sanders (Fellow, IEEE) received the S.B. degree in electrical engineering and physics in 1985, and the S.M. and Ph.D. degrees in electrical engineering from the Massachusetts Institute of Technology, Cambridge, MA, USA, in 1985 and 1989, respectively.

He is currently a Professor with the Department of Electrical Engineering and Computer Sciences, University of California, Berkeley, CA, USA, and co-founder and Chief Technology Officer with Amber Kinetics, a Technology Developer and manufacturer of utility scale flywheel energy storage systems. Following an early experience as a Design Engineer with the Honeywell Test Instruments Division from 1981 to 1983, he joined the UC Berkeley faculty in 1989. His technical interests are broadly in electrical energy and power conversion systems. He is presently or has recently been active in supervising research projects in the areas of renewable energy systems, high frequency integrated power conversion circuits, IC designs for power conversion applications, and electric machine systems. During the 1992–1993 academic year, he was on industrial leave with National Semiconductor, Santa Clara, CA.

Dr. Sanders was the recipient of the NSF Young Investigator Award and multiple Best Paper Awards from the IEEE Power Electronics and IEEE Industry Applications Societies, and IEEE PELS Modeling and Control Technical Achievement Award. He was the Chair of the IEEE PELS Technical Committee on Computers in Power Electronics, Chair of the IEEE PELS Technical Committee on Power Conversion Components and Systems, and as Member-At-Large of the IEEE PELS Adcom. He is a past Distinguished Lecturer of the IEEE PELS and IAS societies.

Robert Carl Nikolai Pilawa-Podgurski (Senior Member, IEEE) received the B.S., M.Eng., and Ph.D. degrees from MIT, Cambridge, MA, USA, in 2005, 2007, and 2012, respectively.

He was born in Hedemora, Sweden. He is currently an Associate Professor with the Electrical Engineering and Computer Sciences Department, University of California, Berkeley, CA, USA. Previously, he was an Associate Professor in electrical and computer engineering with the University of Illinois Urbana-Champaign. He performs research in the area of power electronics. He has coauthored 11 IEEE prize papers. His research interests include renewable energy applications, electric vehicles, CMOS power management, high density and high efficiency power converters, datacenter power delivery, and advanced control of power converters.

Dr. Pilawa-Podgurski was the Student Activities Chair for IEEE Energy Conversion Congress and Exposition 2016 and 2017, and the Technical Co-Chair for the 4th IEEE Workshop on Wide Bandgap Power Devices and Applications, 2016. Since 2014, he has been the PELS Technical Committee 6-Emerging Power Electronics Technologies as Awards Chair, Secretary, Vice Chair, and (presently) Chair. From 2016 to 2019, he was the Chair of PELS Technical Committee 2-Power Conversion Systems and Components. From 2014 to 2019, he was an Associate Editor for the IEEE TRANSACTIONS ON POWER ELECTRONICS and IEEE JOURNAL OF EMERGING AND SELECTED TOPICS IN POWER ELECTRONICS. Since 2018, he has been a Member of the ISSCC Power Management Committee. He was the recipient of the Chorafas Award for outstanding MIT EECS Master's thesis, the Google Faculty Research Award in 2013, and 2014 Richard M. Bass Outstanding Young Power Electronics Engineer Award of the IEEE Power Electronics Society, given annually to one individual for outstanding contributions to the field of power electronics before the age of 35. In 2015, he was also the recipient of the Air Force Office of Scientific Research Young Investigator Award, the UIUC Dean's Award for Excellence in Research in 2016, UIUC Campus Distinguished Promotion Award in 2017, and UIUC ECE Ronald W. Pratt Faculty Outstanding Teaching Award in 2017, and he was the 2018 recipient of the IEEE Education Society Mac E. Van Valkenburg Award given for outstanding contributions to teaching unusually early in ones career in 2018.